

## Nonhydrostatic Atmospheric Models and Operational Development at JMA

Kazuo SAITO

*Meteorological Research Institute, Tsukuba, Japan*

**Jun-ichi ISHIDA, Kohei ARANAMI, Tabito HARA, Tomonori SEGAWA,  
Masami NARITA and Yuuki HONDA**

*Numerical Prediction Division, Japan Meteorological Agency, Tokyo, Japan*

*(Manuscript received 27 November 2006, final form 3 April 2007)*

### Abstract

This paper reviews nonhydrostatic atmospheric models for research and NWP. Classification of nonhydrostatic atmospheric models and numerical methods to treat sound waves are described with their relative advantages. The current operational nonhydrostatic NWP models at various forecast centers and community nonhydrostatic models for research are reviewed.

Brief history and development of the JMA nonhydrostatic model, a community mesoscale model for research and NWP in Japan, is introduced. Current status and near future plans of the operational nonhydrostatic mesoscale model at JMA are presented.

### 1. Introduction

Attempt to quantitatively predict the state of future atmosphere based on the physical laws such as the fluid dynamics and thermodynamics was started with the Richardson's dream in 1920's, and more than a half century has passed since the Charney's historical first success of the numerical weather prediction (NWP). During these 85 years, the atmospheric models have evolved from the approximated models such as the barotropic models to less filtered models to improve their accuracy. Primitive models applied to the practical use in early 1970's had made a brilliant success in the NWP fields from regional predictions to global gen-

eral circulations. However, primitive models possess the approximation which replaces the vertical momentum equation with the relationship of hydrostatic equilibrium thus cannot be applied to the simulation of small scale phenomena where the aspect ratio approaches unity. To meet the expectations to the prediction of local meteorology, horizontal resolutions of operational mesoscale models in world main forecast centers have been becoming higher, and are approaching several kilometers, the limit of validity of the hydrostatic approximation.

Nonhydrostatic models were initially developed as a research tool for small scale meteorological phenomena such as convection or nonlinear mountain waves. Today, several nonhydrostatic models have been developed and are applied to numerical simulations and operational NWP. Following the UK Met Office (UKMO) and the Deutscher Wetterdienst (DWD) of Germany, the Japan Meteorological

---

Corresponding author: Kazuo Saito, Second Laboratory, Forecast Research Department, Meteorological Research Institute, 1-1 Nagamine, Tsukuba, Ibaraki 305-0052, Japan.  
E-mail: ksaito@mri-jma.go.jp  
© 2007, Meteorological Society of Japan

Agency (JMA) started its operational run of a nonhydrostatic mesoscale model in 2004. The National Center for Environmental Prediction (NCEP) of USA began running nonhydrostatic models for high resolution windows in 2004 and full-scale regionals run in 2006. The China Meteorological Administration (CMA) also started operational run of their nonhydrostatic models for regional predictions in 2006. In this paper, we review the basic concept of the nonhydrostatic model and current nonhydrostatic atmospheric models for research and NWP. Brief history, recent development as for the JMA nonhydrostatic model are also presented with the near future plans.

## 2. Classification of nonhydrostatic models

### 2.1 Basic equations

State of dry air can be expressed by temperature ( $T$ ), pressure ( $p$ ), density ( $\rho$ ), and three components of wind ( $u, v, w$ ). As the physical laws, momentum equations in the three directions, the continuity equation, the thermodynamic equation and the state equation compose six basic equations corresponding to the six variables. Neglecting the Coriolis force and terms relating to the earth's curvature and diffusion, they are written as

$$\frac{d\mathbf{v}}{dt} = -\frac{1}{\rho}\nabla p - g\mathbf{k}, \quad (1.1)$$

$$\frac{dp}{dt} = -\rho\nabla \cdot \mathbf{v}, \quad (1.2)$$

$$\frac{d\theta}{dt} = \frac{Q}{C_p\pi}, \quad (1.3)$$

$$p = \rho RT, \quad (1.4)$$

where  $\mathbf{v}$  is the wind vector,  $g$  the gravity acceleration,  $R$  the gas constant for dry air,  $Q$  the adiabatic heating,  $C_p$  ( $= 7R/2$ ) the specific heat of dry air at constant pressure, and  $\mathbf{k}$  denotes a unit vector in the vertical direction. The Exner function ( $\pi$ ) and the potential temperature ( $\theta$ ) are defined as

$$\pi = \left(\frac{p}{p_0}\right)^{R/C_p}, \quad (1.5)$$

$$\theta = \frac{T}{\pi}, \quad (1.6)$$

where  $p_0$  is the reference pressure (normally 1000 hPa). The momentum equation may be rewritten in the following form using  $C_p$  and  $\pi$ ,

$$\frac{d\mathbf{v}}{dt} = -C_p\theta\nabla\pi - g\mathbf{k}. \quad (1.1')$$

Using the relation

$$\frac{dA}{dt} = \frac{\partial A}{\partial t} + \mathbf{v} \cdot \nabla A, \quad (1.7)$$

the continuity equation (1.2) and the total differentiation can be written in the flux form as

$$\frac{\partial \rho}{\partial t} + \nabla \cdot (\rho\mathbf{v}) = 0, \quad (1.8)$$

$$\rho \frac{dA}{dt} = \frac{\partial \rho A}{\partial t} + \nabla \cdot (\rho A\mathbf{v}). \quad (1.9)$$

Using (1.9), the momentum equation (1.1) can be rewritten in the flux form as

$$\frac{\partial \rho\mathbf{v}}{\partial t} + \mathbf{adv} + \nabla p = -\rho g\mathbf{k}, \quad (1.10)$$

where  $\mathbf{adv}$  is the advection in the flux form, whose components in the  $x$ ,  $y$  and  $z$  directions are obtained by substituting  $u$ ,  $v$ , and  $w$  for  $A$  in the second term of *r.h.s.* of (1.9), respectively.

In the hydrostatic approximation, the vertical momentum equation is replaced by the following relationship of the hydrostatic equilibrium,

$$\frac{\partial p}{\partial z} = -\rho g. \quad (1.11)$$

### 2.2 Classification of nonhydrostatic models with the continuity equation

#### a. Anelastic model

The anelastic (AE) model removes sound waves from solutions in the equation system by a scale analysis (Ogura and Phillips 1962). Field variables are divided into the time independent horizontal uniform reference state  $\bar{\phi}(z)$  and its perturbation  $\phi'(x, y, z, t)$  as

$$p = \bar{p} + p', \quad \rho = \bar{\rho} + \rho', \quad \theta = \bar{\theta} + \theta'. \quad (1.12)$$

Substituting the reference density in the momentum and continuity equations, we obtain

$$\frac{\partial \bar{\rho}\mathbf{v}}{\partial t} + \mathbf{Adv} + \nabla p' = -\rho' g\mathbf{k}, \quad (1.13)$$

$$\nabla \cdot (\bar{\rho}\mathbf{v}) = 0, \quad (1.14)$$

where the hydrostatic equilibrium is assumed for the reference atmosphere, and  $\mathbf{Adv}$  is the flux form advection term where the reference density is used.

From the state equation, the density perturbation can be divided into the perturbation of potential temperature and pressure as

$$\rho' = -\rho \frac{\theta'}{\theta} + \rho \frac{C_v}{C_p} \frac{p'}{p} = -\rho \frac{\theta'}{\theta} + \frac{p'}{C_S^2} \quad (1.15)$$

where  $C_v$  ( $= 5R/2$ ) is the specific heat of dry air at constant volume and  $C_S$  the speed of sound waves. Using (1.15), the momentum equation can be written as

$$\frac{\partial \bar{\rho} \mathbf{v}}{\partial t} + \mathbf{Adv} + \nabla p' + \frac{p'}{C_S^2} \mathbf{g} \mathbf{k} = \bar{\rho} \frac{\theta'}{\theta} \mathbf{g} \mathbf{k}. \quad (1.16)$$

If the Exner function is used to represent the pressure, the equation (1.1') takes the following form

$$\frac{d\mathbf{v}}{dt} + C_p \bar{\theta} \nabla \pi' = \frac{\theta'}{\bar{\theta}} \mathbf{g} \mathbf{k}, \quad (1.16')$$

where the pressure perturbation term does not appear in the vertical momentum equation.

If we assume the constant density  $\rho_0$ , the momentum and continuity equations are further reduced to the following equations for an incompressible flow or the Boussinesq atmosphere.

$$\frac{d\mathbf{v}}{dt} + \frac{1}{\rho_0} \nabla p' = \frac{\theta'}{\bar{\theta}} \mathbf{g} \mathbf{k}, \quad (1.17)$$

$$\nabla \cdot \mathbf{v} = 0. \quad (1.18)$$

The anelastic approximation is available for most mesoscale atmospheric simulations and had been widely used in several research models. However, the anelastic approximation of the continuity equation presumes the mass conservation in the model domain thus AE models cannot express variation of the horizontal mean pressure. This approximation also removes the thermal expansion of air.

Durrant (1989) suggested a 'pseudo-incompressible approximation' as an improvement form of the anelastic continuity equation to incorporate the effect of the thermal expansion of air, assuming that perturbation pressure is negligible to the reference pressure,

$$\nabla \cdot (\bar{\rho} \bar{\theta} \mathbf{v}) = \frac{H}{C_p \bar{\pi}}, \quad (1.19)$$

where  $H$  ( $= \rho Q$ ) is the rate of heating per unit volume.

As discussed in the next subsection, AE scheme needs a 3 dimensional elliptic pressure equation solver. Typical examples of the anelastic model are Sommeria (1976), Clark (1977) and Soon and Ogura (1980).

### b. Quasi compressible model

The quasi-compressible model considers the compressibility of air and predicts the pressure from divergence, while the reference density is used for momentum equations. The equation of state does not appear since the time tendency of density is not explicitly considered. The continuity equation formally takes the following form

$$\frac{\partial \rho}{\partial t} + \nabla \cdot (\bar{\rho} \mathbf{v}) = 0. \quad (1.20)$$

Using the relation of (1.15), following pressure equation is obtained

$$\frac{\partial p}{\partial t} = -\bar{C}_S^2 \left\{ \nabla \cdot (\bar{\rho} \mathbf{v}) - \frac{\bar{\rho}}{\bar{\theta}} \frac{\partial \theta}{\partial t} \right\}, \quad (1.21)$$

and if the Exner function is used to represent the pressure, the pressure equation is given by

$$\frac{d\pi}{dt} = -\frac{R\pi}{C_v} (\nabla \cdot \mathbf{v}) + \frac{C_S^2}{C_p \bar{\theta}^2} \frac{d\theta}{dt}. \quad (1.21')$$

The *r.h.s.* of (1.21) and (1.21') consist of the divergence and the thermal expansion of air. Momentum equation is same<sup>1</sup> as in the anelastic equation, (1.16) or (1.16').

The quasi-compressible model includes sound waves in its solutions, however the accuracy is almost same as in the anelastic model due to the linearization. Typical examples of the quasi-compressible model are Klemp and Wilhelmson (1978), Pielke et al. (1992), Xue et al. (1995) and Tsuboki and Sakakibara (2002).

### c. Fully compressible model

The fully compressible model uses the compressible continuity equation (1.2) or (1.8), and the linearization with the reference atmosphere is not employed. Since the fully compressible

1 Quasi compressible continuity equation (1.20) does not satisfy the relation (1.9), thus strictly speaking momentum equations cannot be written in the flux form. This error may cause a computational instability. (Yoshizaki 1988; Saito 1999).

Table 1. Classification of nonhydrostatic models and their behaviors.

Classification	Adiabatic expansion			Constant volume heating		Constant pressure heating	
	Pressure	Density	Volume	Pressure	Density	Volume	Density
Anelastic (AE)	impossible			invariant	invariant	invariant	invariant
Quasi-compressible without the thermal expansion term	decrease	invariant	increase	invariant	invariant	invariant	invariant
Quasi-compressible with the thermal expansion term	decrease	invariant	increase	increase	invariant	increase	invariant
Fully-compressible without the thermal expansion term	decrease	decrease	increase	invariant	decrease	invariant	decrease
Fully-compressible with the thermal expansion term	decrease	decrease	increase	increase	invariant	increase	decrease

model includes sound waves in its solutions and allows the time change of the density, careful attentions must be paid not only on computation of sound waves but on computational accuracy and the finite discretization because consideration of time change of the density sometimes causes a problem of mass conservation. Tapp and White (1976) was the first fully compressible mesoscale nonhydrostatic model while current most NWP nonhydrostatic models (see Table 3) use the fully compressible equations.

Table 1 shows the classification of nonhydrostatic models and their behaviors against manipulations. In the fully compressible system, the pressure and the density decrease for adiabatic expansion when the volume increases. The anelastic system does not express the manipulation of expansion because it is inherently incompressible. In the quasi-compressible system, the pressure decreases but the density is not changed.

Another point which deserves comment is the treatment of the thermal expansion term in the pressure equation. In this table, in addition to the three types of the nonhydrostatic model, classifications are made by the consideration of the thermal expansion, because some nonhydrostatic models (e.g., Klemp and Wilhelmson 1978; Pielke et al. 1992; Dudhia 1993; Doms

and Schaettler 1997) omit this term to avoid numerical problems. However, this term represents a substantial part of the state equation and is important to evaluate density perturbation accurately. As shown in Table 1, even in the fully compressible model, behaviors to diabatic heating differ with and without the thermal expansion term in the pressure equation. If this term is omitted, increase of pressure is not expressed for constant volume heating, and increase of volume is not expressed for constant pressure heating. Klemp and Wilhelmson (1978) concluded that the thermal expansion term in the pressure equation was negligible since its inclusion yielded only trivial differences in results except averaged pressure change less than 0.5 hPa. Dudhia (1993) excused that in a model with a rigid upper boundary neglecting this term may be suitable to avoid the overestimation of atmospheric heating. However Klemp and Wilhelmson's (1978) result was for the one hour simulation. Omitting this term may cause problems in longer period numerical weather prediction and the associated data assimilation cycle.

### 2.3 Pressure equation and treatment of sound waves

As described in the previous section, nonhydrostatic models are classified into anelastic

models and compressible (elastic) models. In terms of the treatment of sound waves, compressible models can be classified further. In the following discussion, a set of flux form equations is assumed<sup>2</sup>. The momentum equation can be written in the form of

$$\frac{\partial \mathbf{V}}{\partial t} + (\nabla + h\mathbf{k})P = \mathbf{FV}, \quad (1.22)$$

where  $\mathbf{V} = \rho\mathbf{v}$ ,  $P = p'$ ,  $h = g/C_s^2$ , and  $\mathbf{FV}$  is the forcing term which consists of advection and buoyancy. For anelastic and quasi-compressible models, the reference density is used for  $\mathbf{V}$ . Continuity equation in the anelastic model is

$$\nabla \cdot \mathbf{V} = 0, \quad (1.23)$$

while in the compressible model, the pressure equation is

$$\frac{\partial P}{\partial t} + C_S^2(\nabla \cdot \mathbf{V}) = FP, \quad (1.24)$$

where  $FP$  is the forcing term, such as the time tendency of the potential temperature.

#### a. AE scheme

Taking total divergence of (1.22) yields the following 3-dimensional Poisson-type pressure diagnostic equation

$$\nabla^2 P + \frac{\partial}{\partial z}(hP) = FP.AE, \quad (1.25)$$

where *r.h.s.* is the forcing term,

$$FP.AE = \nabla \cdot \mathbf{FV} - \frac{\partial}{\partial t}(\nabla \cdot \mathbf{V}). \quad (1.26)$$

The second term must be zero in the continuity equation (1.23), while is often replaced by the total divergence computed in the former time steps to maintain the computational stability (Clark 1977).

#### b. HI-VI scheme

The HI-VI (horizontally implicit vertically implicit) scheme treats sound waves implicitly for both vertical and horizontal directions. This scheme, often referred as the *semi-implicit* method, was first implemented by Tapp and White (1976). For (1.22) and (1.24), the momentum and pressure equations are as follows

$$\frac{\partial \bar{\mathbf{V}}}{\partial t} + (\nabla + h\mathbf{k})\bar{P}^t = \mathbf{FV}, \quad (1.27)$$

$$\frac{\partial \bar{P}}{\partial t} + C_S^2(\nabla \cdot \bar{\mathbf{V}}^t) = FP, \quad (1.28)$$

where over bar with superscript  $t$  expresses a weighted time averaged value defined by

$$\bar{A}^t = \frac{1 + \alpha}{2} A^{t+\Delta t} + \frac{1 - \alpha}{2} A^{t-\Delta t}. \quad (1.29)$$

Here,  $\alpha$  is a weight parameter which determines the implicit rate<sup>3</sup>. Assuming a centered time discretization

$$\frac{\partial A}{\partial t} = \frac{A^{t+\Delta t} - A^{t-\Delta t}}{2\Delta t}, \quad (1.30)$$

and introducing an operator for  $\mathbf{V}$  and  $P$

$$A' = \bar{A}^t - A^t, \quad (1.31)$$

(1.27) and (1.28) can be rewritten as

$$\frac{\mathbf{V}'}{(1 + \alpha)\Delta t} + (\nabla + h\mathbf{k})P' = \mathbf{FV}', \quad (1.32)$$

$$\frac{P'}{(1 + \alpha)\Delta t} + C_S^2(\nabla \cdot \mathbf{V}') = FP', \quad (1.33)$$

where

$$\mathbf{FV}' = \mathbf{FV} - \frac{\mathbf{V}^t - \mathbf{V}^{t-\Delta t}}{(1 + \alpha)\Delta t} - (\nabla + h\mathbf{k})P^t, \quad (1.34)$$

$$FP' = FP - \frac{P^t - P^{t-\Delta t}}{(1 + \alpha)\Delta t} - C_S^2(\nabla \cdot \mathbf{V}^t). \quad (1.35)$$

Taking divergence of (1.32), the following 3-dimensional Helmholtz-type pressure equation is obtained

$$\nabla^2 P' + \frac{\partial}{\partial z}(hP') + eP' = FP.HI, \quad (1.36)$$

where

$$e = -\frac{1}{((1 + \alpha)\Delta t C_S)^2}, \quad (1.37)$$

$$FP.HI = \nabla \cdot \mathbf{FV}' - \frac{FP'}{(1 + \alpha)\Delta t C_S^2}. \quad (1.38)$$

The pressure equation (1.36) is formally similar to the anelastic pressure equation (1.25).

2 Similar discussion can be applied to the model which uses advective form equations (1.16') and (1.21'). For the detail, see Steppeler et al. (2003a).

3 Tapp and White used  $\alpha = 0$ , while  $\alpha = 0.5$  is used in the JMA nonhydrostatic model. See Section 2.4.

c. *HE-VI scheme*

The HE-VI (horizontally explicit vertically implicit) scheme treats sound waves implicitly only for the vertical direction. This scheme was first developed by Klemp and Wilhelmson (1978), and often referred as the split-explicit method because sound waves are treated in a short time step while low frequency modes and physical processes are treated in a long time step. For (1.22) and (1.24), the momentum and pressure equations are as follows with the forward time integration of horizontal momentum equations and the backward integration of vertical and pressure equations,

$$\frac{\partial U}{\partial t} + \frac{\partial P}{\partial x} = FU, \quad (1.39)$$

$$\frac{\partial V}{\partial t} + \frac{\partial P}{\partial y} = FV, \quad (1.39')$$

$$\frac{\partial W}{\partial t} + \left( \frac{\partial}{\partial z} + h \right) \bar{P}^\tau = FW, \quad (1.40)$$

$$\frac{\partial P}{\partial t} + C_S^2 (\nabla \cdot \bar{\mathbf{V}}^\tau) = FP, \quad (1.41)$$

where over bar with superscript  $\tau$  expresses a weighted time averaged value defined by

$$\bar{A}^\tau = \frac{1+\beta}{2} A^{\tau+\Delta\tau} + \frac{1-\beta}{2} A^\tau. \quad (1.42)$$

Here,  $\beta$  is a weight parameter which determines the implicit rate<sup>4</sup>. Assuming a two time level discretization<sup>5</sup>

$$\frac{\partial A}{\partial t} = \frac{A^{\tau+\Delta\tau} - A^\tau}{\Delta\tau}, \quad (1.43)$$

and eliminating  $W^\tau$ , the following 1-dimensional Helmholtz pressure equation is obtained

$$\frac{\partial^2 \bar{P}^\tau}{\partial z^2} + \frac{\partial}{\partial z} (h \bar{P}^\tau) + e' \bar{P}^\tau = FP.HE, \quad (1.44)$$

where

$$e' = - \left\{ \frac{2}{(1+\beta)\Delta\tau C_S} \right\}^2, \quad (1.45)$$

$$\begin{aligned} FP.HE = & - \frac{2}{(1+\beta)\Delta\tau} \frac{FP}{C_S^2} + \frac{\partial}{\partial z} FW \\ & + \frac{2}{(1+\beta)\Delta\tau} \left\{ \left( \frac{\partial \bar{U}^\tau}{\partial x} + \frac{\partial \bar{V}^\tau}{\partial y} \right) + \frac{\partial W^\tau}{\partial z} \right\} \\ & + e' P^\tau. \end{aligned} \quad (1.46)$$

The pressure equation (1.44) is formally similar to the pressure equation of the HI-VI scheme (1.36) except the Laplacian in the pressure equation is vertically 1-dimensional.

#### 2.4 Relative advantages in three methods

Here we briefly discuss relative advantages in above mentioned three numerical methods in the nonhydrostatic model.

As for the accuracy, AE scheme includes the approximation of incompressibility and linearization of basic equations with the reference state. These approximations have little influences in most cloud scale simulations. However, neglecting of compressibility assumes the preservation of total mass in the model domain, and this assumption is not necessarily assured in large scale computations. Beside, deviation from the horizontal homogeneous reference state becomes large when the model domain is large. No special approximations are included in HI-VI and HE-VI schemes in principle. Implicit treatment of gravity waves may deform meteorologically meaningful gravity waves in HI-VI scheme if a very large time step was chosen. In HE-VI scheme, the acoustic filter which damps the divergence to attenuate sound waves is often required in momentum equations (Skamarock and Klemp 1992). It seems both points yield no practical errors in the prediction of mesoscale meteorological phenomena.

Computational robustness is generally good in AE scheme because sound waves are removed from its solution. In HI-VI scheme, most models treat only the basic state implicitly thus computational problem may arise in case perturbation from the basic state becomes large. The linear stability analysis for sound waves for HI-VI scheme without orography was given by Tapp and White (1976) for the case of  $\alpha = 0$ . They showed that a stability criterion is  $\Delta t < 1/N$ , where  $N$  is the Brunt-Vaisala frequency. Ikawa (1988) made a stability analysis with orography and showed that  $\alpha > 0$  is needed when orography is incorpo-

<sup>4</sup> Usually  $\beta = 1$  is used.

<sup>5</sup> A three time level scheme may be applicable in the short time step integration. The JMA nonhydrostatic model has an optional choice to use the leap-frog scheme for time splitting of gravity waves.

rated, and for a very steep mountain HI-VI scheme becomes unstable no matter what value of  $\alpha$  is chosen. His suggestion was confirmed by the Steep Mountain Model Intercomparison Project (St-MIP) by Satomura et al. (2003). They showed that with the terrain-following coordinates, HI-VI scheme faced instability in a very steep mountain case where the slope angle exceeds 26.5 degree, while HE-VI scheme could complete the time integration<sup>6</sup>. This instability in HI-VI scheme does not cause a serious problem in the ordinary mesoscale NWP with a horizontal resolution of a few kilometers where very steep orography is not included.

Skamarock and Klemp (1992) conducted a stability analysis of the interaction between acoustic modes and advection in HE-VI scheme. They showed that weak instability regions arise when the number of small time step is increased but the instability can be removed by a time filter (Robert 1966). They also proposed a divergence filter which damps acoustic mode and improves the stability when the implicit rate is small.

The difference of pressure equations characterizes the advantage and disadvantage among the three methods. In HE-VI scheme, the elliptic pressure equation (1.44) is one-dimensional and is easily solved by the Gaussian elimination. Scalability is good for parallel computing because all-to-all inter-node communication is not required. Since the elliptic pressure equations of AE and HI-VI schemes ((1.25) and (1.36)) are 3-dimensional, efficiency of these models depend on the numerical solver for the elliptic equation.

One choice is the use of a direct method such as the dimension reduction method (Ogura 1969). Ikawa and Saito (1991) used a direct method with an iterative procedure for their AE scheme. Saito (1997) applied the direct method to HI-VI scheme and removed the iterative procedure when the surface friction is incorporated. The dimension reduction method

employs eigen function transform, which is interpreted as a kind of a spectral method. The computation in the operation of tensor product increases proportionally to the third power of the model size  $N$  (grid number in each direction). In this point of view, spectral method is applicable to the HI-VI scheme and has been employed in some HI-VI models (e.g., Juang 2000; Goda and Kurihara 1991). The double Fourier transform decreases the computational amount from  $N^3$  to  $N^2 \log(N)$  with FFT, however, inter-node communication is required thus the 3-dimensional elliptic equation is still a drawback for a large scale computation in parallel computing architectures.

Another choice is the use of iterative solvers for the elliptic equation. Since the conventional successive over relaxation (SOR) scheme is not suitable for parallel computation, the parallel SOR (PSOR) method has been proposed by Xie and Adams (1999). Current common methods in NWP models are the conjugate gradient method or conjugate residual method with appropriate preconditioners (e.g., Kapitza and Eppel 1987; Ajmani et al. 1994). A generalized conjugate residual method is used in UM of UK Met Office (Staniforth et al. 2002). Multi-grid methods (Douglas 1992) have been proposed to reduce the inter-node communication. Ishii and Kurihara (2002) tested PSOR and multi-grid methods by applying them to the JMA ocean model, and reported that the multi-grid method was faster than PSOR method in a large scale parallel computation.

To further relax the integration time step constraint in HI-VI scheme, implicit treatment of gravity waves (e.g., Cullen 1990) is often combined with a Lagrangian treatment of advection (e.g., Tanguay 1990; Golding 1992; Benoit et al. 1997). This method, the semi-implicit semi-Lagrangian (SI-SL) scheme is often employed for global-regional unified NWP models (see Section 3). In case of HE-VI scheme, horizontally propagating sound waves may be detrimental to implement the semi-Lagrangian scheme.

Table 2 summarizes the comparisons of the three methods. Relative efficiency may depend on the computer architectures. Considering the inter-node communication in HI-VI scheme, HI-VI scheme may be suitable for vector processor computers while HE-VI scheme is more

<sup>6</sup> Another important indication by Satomura et al. (2003) is that contrary to the presumption, the use of terrain-following coordinates does not cause a clear error on the results of mountain wave simulation even in the steepest mountain case. They concluded that the  $z^*$  terrain-following coordinates can be employed in high resolution models which contain steep slopes about 45 degree.

Table 2. Comparison of numerical methods for nonhydrostatic model.

Method	Accuracy	Computational robustness	Pressure equation	Scalability in parallel computation	Efficiency in large scale computation	Compatibility with semi-Lagrangian scheme	Compatibility with spectral method
AE	Anelastic approximation	Good	3D Poisson	Depends on elliptic solver	Depends on elliptic solver	Good	Good
HI-VI	Good	Fair	3D Helmholtz	Depends on elliptic solver	Depends on elliptic solver	Good	Good
HE-VI	Good	Fair	1D Helmholtz	Good	Good	Sound waves exist	Fair

appropriate to massive parallel scalar computers. Saito et al. (1998) made a comparison of computational times between HI-VI scheme of MRI-NHM and HE-VI scheme of LM at DWD on the DWD's CRAY super computer. They reported that a rough yardstick which determines the comparative efficiency of the two models was given by the relative magnitude between the Courant number for sound wave speed and the number of iterative procedures in the elliptic pressure equation solver in HI-VI scheme. Thomas et al. (2000) implemented a HI-VI scheme in LM, while reported that HE-VI scheme was more efficient for limited area NWP applications. Similar tendency can be seen in the comparison between HE-VI and HI-VI schemes in the JMA nonhydrostatic model. However in their results, reduction of computer time with the semi-Lagrangian scheme was not considered.

Compatibility with high-order time and space discretization schemes may be better in HE-VI schemes, because in HI-VI scheme the 3-dimensional pressure equation must be discretized in a matrix form to apply the numerical solver. Comparison of HE-VI and HI-VI schemes have not been made fully, and more systematic intercomparison should be conducted.

### 3. Nonhydrostatic models for NWP and research

#### 3.1 Nonhydrostatic NWP models at operational centers

Table 3 summarizes nonhydrostatic NWP models in main forecast centers. As of Septem-

ber 2006, five nonhydrostatic models (UM, LM, JMA-NHM, WRF-NMM and GRAPES) have been used for full-scale regional predictions at UKMO, DWD, JMA, NCEP and CMA, respectively. WRF-ARW has been employed for weather predictions in the limited area high resolution windows over US and for some members in the short range ensemble forecast system (SREF) at NCEP. Canadian GEM and NCEP RSM have been operated using hydrostatic dynamics, while they have nonhydrostatic options.

#### a. UK Met Office

UKMO was the first operational center which implemented a nonhydrostatic model for operational NWP. The UKMO Mesoscale Model (Golding 1990) was introduced in 1985 with a resolution of 15 km L16. The model was originated from the Tapp and White (1976) HI-VI model with the inclusion of orography by Carpenter (1979). Vertical resolution was enhanced to L32 in 1990. Although this mesoscale model was replaced with the hydrostatic Unified model (UM; Cullen 1993), a SI-SL nonhydrostatic version of UM (new dynamics; Staniforth et al. 2002) was implemented and has been used for operational NWP since August 2002 (Davies et al. 2005). The current UM operational specification is  $0.5625 \text{ deg} \times 0.375 \text{ deg}$  (about 40 km) L50 for a global model and 12 km L38 for North Atlantic and Europe (NAE) area (Fig. 1). Since UM does not have a hydrostatic option, both regional and global computations are done with the nonhydrostatic dynamics, and this is the first operational im-

Table 3. Nonhydrostatic NWP models (as of November 2006).

Model	Country (Forecast center)	Method	Full operation	Domain and Resolution	References
UKMO Mesoscale Model	UK (UKMO)	HI-VI	1985–1993	UK 15 km L32	Tapp and White (1976) Carpenter (1979) Golding (1990)
UM	UK (UKMO)	SI-SL	Aug 2002–	Global 40 km L50 NAE 12 km L38 UK 4 km L38	Cullen (1993) Staniforth et al. (2002) Davies et al. (2005)
LM	Germany (DWD)	HE-VI	1997–	Europe 7 km L40 (Germany 2.8 km in 2007)	Doms and Schaeffler (1997) Steppeler et al. (2003b; 2006)
JMA-NHM	Japan (JMA, MRI)	HE-VI (HI-VI option)	Sep 2004–	Japan and its surroundings 5 km L50	Ikawa and Saito (1991) Saito et al. (2001; 2006)
WRF-NMM	USA (NCEP)	HE-VI	June 2006– (Nov 2004– for HiRes Window, 2005– for SREF)	North America 12 km L60 SREF 40 km L50 (3 members)	Janjic (2001; 2003)
WRF-ARW	USA (NCAR)	HE-VI	Nov 2004– for HiRes Window 2005– for SREF	SREF 45 km L35 (3 members)	Skamarock et al. (2005) Klemp et al. (2007) Skamarock and Klemp (2007)
RSM	USA (NCEP)	HI-VI (Spectral)	1997– Hawaii (Hydrostatic option)	SREF 40 km L28 (5 members) Hawaii 10 km L40	Juang (2000) Juang et al. (1997)
GEM	Canada (MSC)	SI-SL	Oct 1998– (Hydrostatic option)	Global 0.3 deg L58 Regional 15 km (0.1375 deg) L58	Tanguay et al. (1990) Cote et al. (1998a,b) Yeh et al. (2002)
GRAPES	China (CAMS)	SI-SL	July 2006–	Meso 30 km L33	Chen and Xue (2003) Chen et al. (2003)
ALADIN-NH	France etc.	HI-VI		9.5 km (Hydrostatic)	Bubnova (1995)
NH HIRLAM	Denmark etc.	HE-VI or SI-SL		0.05–0.5 degree (Hydrostatic)	Mannik and Room (2001) Room et al. (2006)
AROME	France (Meteo-France)	SI-SL			Bouttier (2003) Benard et al. (2005)



Fig. 1. Domain of UKMO North Atlantic and European (NAE) model. Small rectangle indicates the domain of the 4 km nested model. By courtesy of Andrew Lorenc of UKMO.

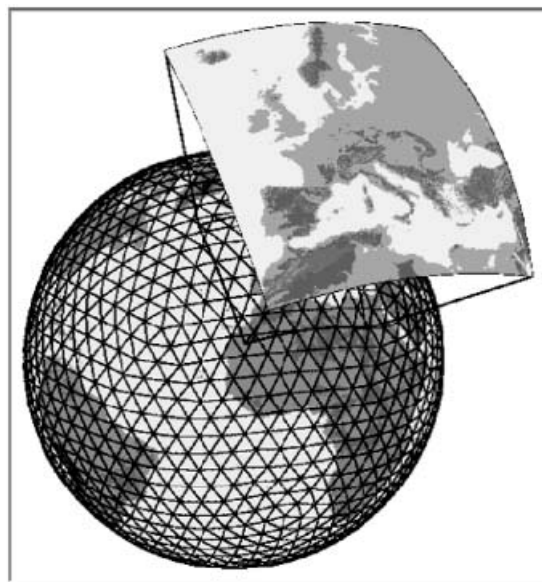


Fig. 2. The icosahedral grid global model GME at DWD and domain of LM. By courtesy of Detlev Majewski of DWD.

plementation of a global nonhydrostatic model. For analysis, 4D-Var has been implemented since October 2004 for the global model and March 2006 for the regional model. Another high resolution nested model which covers UK domain with the resolution of 4 km L38 has been run additionally. A 1.5 km model has been tested in trial mode when severe weather is expected.

UM has been operated at the Thai Meteorological Department, too (34 km horizontal resolution for Southeast Asia and 17 km for Thailand).

#### b. Germany

DWD has been running a nonhydrostatic limited area model LM (Lokal-Modell; Doms and Schaettler 1997) since 1997 with a horizontal resolution of 7 km. Development of LM started in 1995 at DWD and the first version was constructed from DWD's regional model DM (Deutschland Modell) by replacing its hydrostatic solver by a nonhydrostatic dynamical core. Rotated geographical horizontal coordinates and terrain-following vertical coordinates were employed, with a HE-VI treatment of sound and gravity waves. Since September

2005, the number of model levels has been enhanced from 35 to 40 and the domain has been enlarged from  $325 \times 325$  to  $665 \times 667$ . Lateral boundary condition is supplied by the Icosahedral grid global model GME (Majewski et al. 2002) as shown in Fig. 2. For data assimilation, nudging has been employed to initialize LM, where SYNOP, METAR, TEMP, AMDAR and windprofiler data are assimilated. DWD will introduce a high resolution LM (called LMK) which covers Germany and its surroundings with a horizontal resolution of 2.8 km L50 in April 2007. LMK will resolve deep convection explicitly and use radar reflectivity (precipitation scan) via the latent heat nudging technique.

LM has been operated in Italy, Greek and Swiss under COSMO (Consortium of Small scale Modelling) project. A HI-VI version (Thomas et al. 2000) and a very high resolution version using the shaved cell representation of mountains (Steppeler et al. 2006) have also been developed.

#### c. JMA nonhydrostatic model (JMA-NHM)

JMA replaced a hydrostatic spectral meso-scale model with a nonhydrostatic model



Fig. 3. Domain of the JMA mesoscale model (MSM; inner rectangle). Outer rectangle indicates domain of the JMA regional model (RSM).

(JMA-NHM; Saito et al. 2006) in September 2004. The model covers a domain of  $3600 \text{ km} \times 2880 \text{ km}$  which covers Japan and its surrounding areas (Fig. 3). Since March 2006, the resolution has been enhanced from 10 km L40 to 5 km L50. Lateral boundary condition is supplied by the JMA hydrostatic regional spectral model (RSM) whose horizontal resolution is 20 km. As for data assimilation, the Meso 4D-Var (Koizumi et al. 2005) has been implemented since March 2002, and a similar 4D-Var system has been implemented to regional analysis since June 2003. Although these 4D-Var systems are currently based on the hydrostatic spectral model, a nonhydrostatic mesoscale 4D-Var system is under development.

JMA-NHM was put into trial operation at the Hong Kong Observatory (HKO) with a horizontal resolution of 5 km and 45 vertical levels in April 2004. It was upgraded in April 2005 to run on an hourly basis to provide rapidly updated quantitative precipitation forecast (QPF) to blend with the radar nowcasting products in RAPIDS (Rainstorm Analysis and Prediction Integrated Data-processing System; Li et al. 2005; Wong et al. 2006).

Detail of JMA-NHM and its relevant works are described in Section 4.

#### d. USA

NCEP has been running a regional model 4 times a day (84 hour for 00, 06, 12 and 18

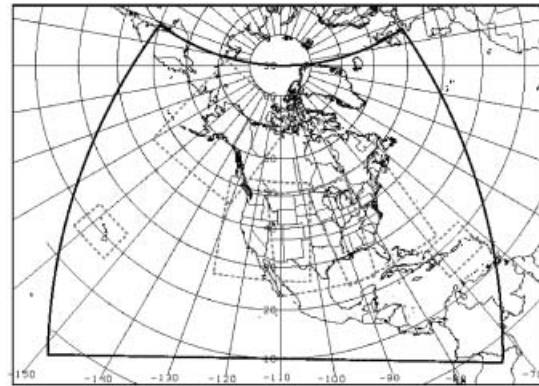


Fig. 4. Domain of NCEP limited area models. The outer domain indicated the domain of NAM. Inner rectangles show the HiRes Window. After NCEP homepage (<http://www.emc.ncep.noaa.gov/>).

UTC) for the NAM (Northern American Mesoscale) domain with a resolution of 12 km L60. In June 2006 the nonhydrostatic WRF-NMM (Weather Research and Forecasting Nonhydrostatic Mesoscale Model; Janjic 2003) replaced the hydrostatic Eta model as the NAM model. The terrain-following, hybrid, hydrostatic pressure-sigma vertical coordinate is used. HE-VI treatment of sound waves is combined with the Adams-Bashforth scheme for horizontal advection and the Crank-Nicholson scheme for vertical advection, which conserves enstrophy, kinetic energy and momentum. A successive assimilation system with 3D-Var called the Grid Statistical Interpolation (GSI) is used.

In the NAM domain, high resolution limited area models have been nested for domains called HiRes Window (Fig. 4). Currently, six domains (Alaska, Hawaii, Puerto Rico, Western US, Central US and Eastern US) are being run. In addition to the WRF-NMM, another version of WRF (WRF-ARW; Advanced Research WRF; Skamarock et al. 2005) and a regional spectral model (RSM; Juang et al. 1997) are employed. WRF-ARW has been developed at NCAR as a successor to MM5 for research and operation. A HE-VI time splitting method using high order schemes in space (fifth order) and time (third order Runge Kutta) are employed with hydrostatic pressure (mass) vertical coordinates. RSM has a nonhydrostatic op-

tion (Juang 2000) but operational run has been done with the hydrostatic dynamics. NCEP also has been developing another SI-SL type non-hydrostatic model (Kar et al. 2005).

NCEP has been operating a short range ensemble forecasting system SREF (Short Range Ensemble Forecasting; Du and Tracton 2001). The current system consists of 10 members of 32 km L60 Eta model, 5 members of 40 km L28 RSM, 3 members of 40 km L50 WRF-NMM and 3 members of 45 km L35 WRF-ARW.

Since 2004 WRF-NMM has been run experimentally with 4.5 km L35 resolution over the eastern three-fourths of the United States (Weiss et al. 2006). A version of the WRF-NMM with multiple moving nests is being developed for hurricane forecasting (Hurricane WRF). This model will replace the current NCEP operational hurricane model in 2007 (Gopalakrishnan et al. 2006).

#### e. Canada

At Environment Canada, Recherche en prévision numérique (RPN) from the Meteorological Research Division, in collaboration with the Canadian Meteorological Centre has developed the SI-SL unified GEM (Global Environmental Multiscale) model (Cote et al. 1998a, 1998b). GEM is a grid-point model and can accommodate a global uniform latitude-longitude grid resolution, a global variable grid resolution, as well as a limited-area grid. Operationally, the variable grid GEM model has been first run in regional mode (Reg-GEM) since February 1997 with a high resolution window of 35 km (0.33 degree) L28 for 48 hour forecasts. In May 2004, the resolution has been increased to 15 km (0.1375 degree) L58. Using a variable grid mesh, the horizontal resolution over Canada is enhanced without lateral boundary conditions (Fig. 5). A 4D-Var data assimilation system (providing initial conditions to the global, uniform grid GEM model for medium-range forecasts) has been implemented in March 2005 for the uniform resolution assimilation cycles, on which a 3D-Var regional spin-up cycle is superimposed to provide initial conditions for up to 48 hour regional forecasts.

Although GEM has a non-hydrostatic option (Yeh et al. 2002), the hydrostatic primitive equations are employed for operational NWP.



Fig. 5. Domain of variable grid GEM at MSC. By courtesy of Jean Cote of RPN.

A nonhydrostatic very high resolution limited-area nested version of GEM (GEM-LAM) has been tested with a horizontal resolution of 2.5 km and down to 250 m.

#### f. China

The National Meteorological Center of China Meteorological Administration (NMC/CMA) started operational run of a limited area non-hydrostatic model GRAPES\_Meso in July 2006 with a resolution of 30 km L33, replacing the CMA's former hydrostatic limited area model. GRAPES (Global/Regional Assimilation Prediction System) is a SI-SL global regional unified model, developed by the Chinese Academy of Meteorological Sciences (CAMS; Chen and Xue 2003; Chen et al. 2003). The latitude longitude spherical coordinate and terrain-following Lorenz type vertical coordinates are employed. A preconditioned generalized conjugate residual method is employed for the 3-dimensional Helmholtz pressure equation solver. CAMS has started a technical cooperation with NCAR since 2002, and GRAPES has a common design with WRF-ARW regarding architecture specific tasks such as I/O functions called driver layer, grid numbering configurations and some parts of physical process packages. CMA is planning to run a global version of GRAPES quasi-operationally in 2007.

*g. ALADIN, HIRLAM and AROME project*

Meteo France has been running a hydrostatic spectral limited area model ALADIN (Aire Limitée Adaptation dynamique Développement Inter-National) for a 2740 km square domain with a resolution of 9.5 km L41. 3D-Var is employed for data assimilation. ALADIN has also been operated in Algeria, Austria, Belgium, Bulgaria, Croatia, Czech Rep., Hungary, Morocco, Poland, Romania, Slovakia, Slovenia and Tunisia with a horizontal resolution 7–31 km. Bubnova et al. (1995) developed an experimental nonhydrostatic version of ALADIN (ALADIN-NH) which uses hydrostatic pressure as the vertical coordinate.

Eight European countries (Denmark, Finland, Iceland, Ireland, Holland, Norway, Spain, and Sweden) have been operating a community hydrostatic limited area model HIRLAM (High Resolution Limited Area Model; Unden et al. 2002) cooperating with Meteo France and ECMWF. These countries are running the model with different domains and resolutions. HIRLAM has two versions, an Euler version and a semi-Lagrangian version. Denmark, Finland and Spain are employing the Euler version while other countries are running the semi-Lagrangian version. Nonhydrostatic versions of HIRLAM (NH HIRLAM) have been presented by Mannik and Room (2001) for the Euler version (HE-VI) and by Room et al. (2006) for the semi-Lagrangian version (SI-SL).

A project developing a nonhydrostatic community NWP model, AROME (Application of Research to Operations at Mesoscale; Bouttier 2003), has been underway. AROME is a SI-SL updated version of ALADIN-NH with physics of the Meso-NH cloud resolving model (Meso-NH; Lafore et al. 1998). Meteo France, as well as several HIRLAM countries, have a plan to introduce AROME with a 2.5 km resolution in 2008 for operational mesoscale NWP.

### 3.2 Nonhydrostatic community models

Table 4 summarizes typical nonhydrostatic community models. Most models in this table were developed as cloud models initially and have been modified for realistic simulations.

Cotton and Tripoli's (1978) cloud model has been extended at Colorado State University (CSU) to the Regional Atmospheric Modeling System (RAMS). RAMS has been widely used

in research fields that includes climate studies to LES. At CSU, RAMS has been used for real time forecasting with 48 km, 12 km and 3 km grid spacing (Cotton et al. 2003). At Wisconsin University, RAMS has been modified to a step mountain model as the University of Wisconsin—Nonhydrostatic Modeling System (<http://cup.aos.wisc.edu/uw-nms.html>).

Klemp and Wilhelmson's (1978) cloud model has been modified at the US Naval Research Laboratory (NRL) to the Coupled Ocean/Atmosphere Mesoscale Prediction System (COAMPS; Hodur 1997). NRL has also been running COAMPS with a horizontal resolution 6 km for the operational typhoon track forecast.

Soong and Ogura's (1980) cloud model has been modified at the NASA Goddard Space Flight Center (GSFC) to the Goddard Cloud Ensemble (GCE) model (Tao and Simpson 1993). The GCE model has been used to simulate many different mesoscale convective systems and to study the role of physical processes in convective systems.

Sommeria's (1976) cloud model has been modified at Meteo France to the Meso-NH model (Lafore 1998) and used for quasi operational NWP. Although the Meso-NH model uses anelastic formula, time change of the horizontal mean pressure is considered by computing the mass flux at lateral boundaries.

Xue et al. (1995) of the Center for Analysis and Prediction of Storms, the Oklahoma University, have developed the Advanced Regional Prediction System (ARPS). ARPS has been applied to many storm scale simulations and was used experimentally in HKO for research and development on local scale prediction. With the ARPS Data Analysis System (ADAS), the Oklahoma University has been run a daily real time analysis and forecast with 27 km, 9 km and 3 km horizontal resolutions.

Tsuboki and Sakakibara (2002) of Nagoya University and the Research Organization for Information Science & Technology (RIST) in Japan have developed the Cloud Resolving Storm Simulator (CReSS). CReSS has been designed to perform cloud to mesoscale simulations on parallel computing facilities. Using the Earth Simulator, a simulation of typhoon with a 1 km horizontal resolution has been successfully performed (Tsuboki 2006).

Some community nonhydrostatic models

Table 4. Cloud models and community nonhydrostatic models.

Model	Main developer	Numerical Method	References	Remarks Website
RAMS	CSU	HE-VI Quasi-compressible	Tripoli and Cotton (1982) Pielke et al. (1992) Cotton et al. (2003)	<a href="http://rams.atmos.colostate.edu/">http://rams.atmos.colostate.edu/</a>
COAMPS	US NRL	HE-VI Quasi-compressible	Klemp and Wilhelmson (1978) Hodur (1997)	<a href="http://www.nrlmry.navy.mil/coamps-web/web/home">http://www.nrlmry.navy.mil/coamps-web/web/home</a>
GCE	NASA/GSFC	AE	Soong and Ogura (1980) Tao and Simpson (1993) Tao (2003)	<a href="http://www.asd.ssc.nasa.gov/m2m/model_report.aspx?model_id=1603">http://www.asd.ssc.nasa.gov/m2m/model_report.aspx?model_id=1603</a>
Meso-NH	Meteo France	AE	Sommeria (1976) Redelsperger and Sommeria (1986) Lafore et al. (1998)	<a href="http://mesonh.aero.obs-mip.fr/mesonh/">http://mesonh.aero.obs-mip.fr/mesonh/</a>
ARPS	CAPS	HE-VI	Xue et al. (1995; 2003)	<a href="http://www.caps.ou.edu/ARPS/index_flash.html">http://www.caps.ou.edu/ARPS/index_flash.html</a>
CRess	Nagoya University, RIST	HE-VI Quasi-compressible	Tsuboki and Sakakibara (2001)	<a href="http://cf.tokyo.rist.or.jp/CRess.top.html">http://cf.tokyo.rist.or.jp/CRess.top.html</a>
MM5	NCAR, PSU	HE-VI	Dudhia (1993) Grell et al. (1994)	<a href="http://www.mmm.ucar.edu/mm5/">http://www.mmm.ucar.edu/mm5/</a>
MC2	RPN	SI-SL	Tanguay et al. (1990) Laprise (1992) Benoit et al. (1997)	<a href="http://www.cccma.ec.gc.ca/models/crcm.shtml">http://www.cccma.ec.gc.ca/models/crcm.shtml</a>

originate from mesoscale models. Dudhia (1993) developed a nonhydrostatic version of the Penn State-NCAR mesoscale model, MM5. Hydrostatic reference state pressure is employed for vertical coordinates. Among the community nonhydrostatic models, MM5 has been most widely used in research fields. In several countries (e.g., Korea, Brazil and China), MM5 has been used as the operational NWP model. A 4D-Var analysis system (Zou et al. 1998) has been developed and opened to the public as a research tool.

Canadian MC2 (Benoit et al. 1997) was developed at RPN. The SI-SL formulation with a terrain-following coordinate was designed for research activities in high resolution weather forecasting. A model based on MC2 has been applied for regional climate modeling at the Climate Research Division at Environment Canada.

These community models are generally well

documented and the source codes are distributed to users on websites. In addition to the models listed in Table 4, several cloud models have been employed for numerical simulations. Formerly, the businesses of cloud models were distinguished from those of operational NWP models. However, recent most mesoscale NWP models are applicable to cloud scale researches as well. Figure 6 shows an example of a cloud resolving simulation by JMA-NHM with a horizontal resolution of 1 km (Eito et al. 2004). Cloud streaks associated with the cold air outbreak over the Sea of Japan in winter are very well reproduced. The border between NWP mesoscale models and community research models has been becoming unclear.

### 3.3 Global nonhydrostatic model

As described in the previous subsection, some forecast centers have been operating/developing global regional unified nonhydro-

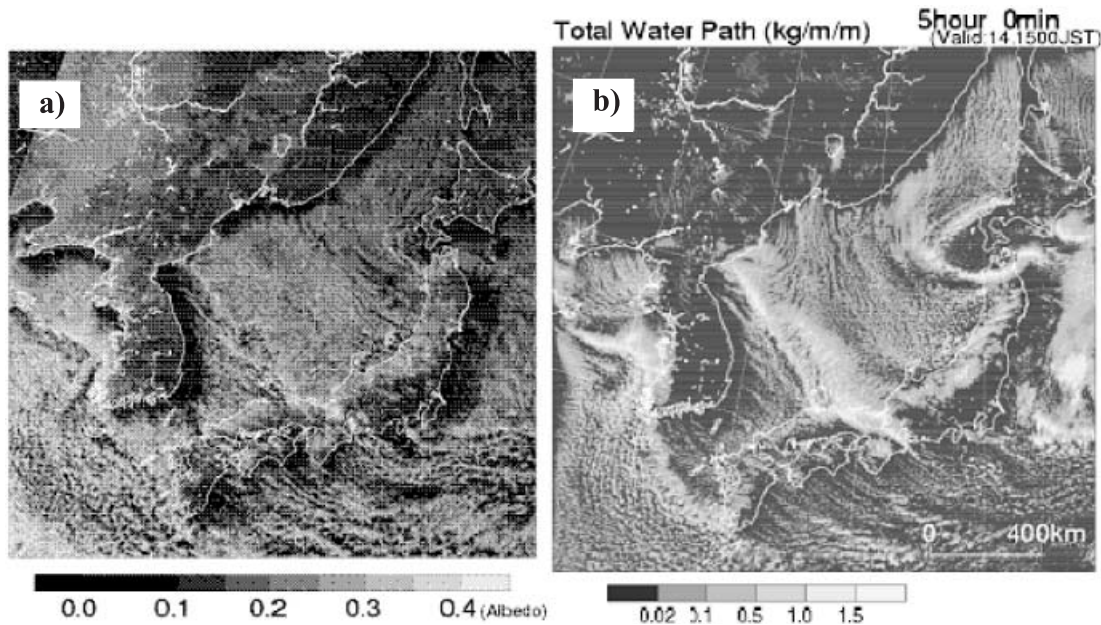


Fig. 6. a) Visible satellite image by GMS-5 at 03 UTC 14 January 2001. b) Corresponding accumulated cloud water predicted by JMA-NHM with a horizontal resolution of 1 km. Five hour forecast from initial time 22 UTC 13 January 2001. After Eito et al. (2004).

static models. One of the merits of the unified model is that a common source programming code can be used for global and regional predictions, which may promote an efficient model development. This merit is important in data assimilation where tangent-linear and adjoint models are required in the 4D-Var system. Another demand is the very high resolution global simulation for climate researches and the future NWP. Although current horizontal resolutions of global models in main forecast centers are several tens of kilometers, they will become less than 10 km in the next few decades. The global cloud resolving simulation may remove the uncertainty of climate models due to the convective parameterization.

In the global nonhydrostatic model, the use of the latitude-longitude grid is faced with the 'pole problem', where grid spacing in the latitudinal direction decreases near poles and the time step is restricted by the CFL condition. Current most common manner in operational NWP models to avoid the pole problem is the SI-SL method. The SI-SL scheme for a global model by Staniforth and Cote (1991) has been evolved to UM of UKMO and GEM of MSC. Other SI-SL global nonhydrostatic models can

be seen in Qian and Semazzi (1988) and GRAPES of CMA. Although relatively large time step can be taken, convergence and efficiency of the elliptic pressure solver may become a problem in a very high resolution case in this type of global model.

Another approach to realize the global nonhydrostatic model is to use quasi-uniform grid configurations on the sphere. The Frontier Research Center for Global Change (FRCGC) of Japan has developed an icosahedral grid nonhydrostatic model NICAM (Nonhydrostatic Icosahedral Atmospheric Model; Tomita and Satoh 2004; Fig. 7a). A global cloud resolving simulation using the Earth Simulator has been conducted with a horizontal resolution of 3.5 km (Satoh et al. 2005). Icosahedral grid global model has been used at DWD for the operational hydrostatic model GME. The Max Planck Institute for Meteorology (MPI-M) and DWD have been developing another icosahedral nonhydrostatic model (ICON-Project; Heinze et al. 2005).

Another type of grid configuration on the sphere, the cubic conformal grid, has been presented by McGregor (1996) and Rancic et al. (1996). Recently, Muroi (2006) developed a

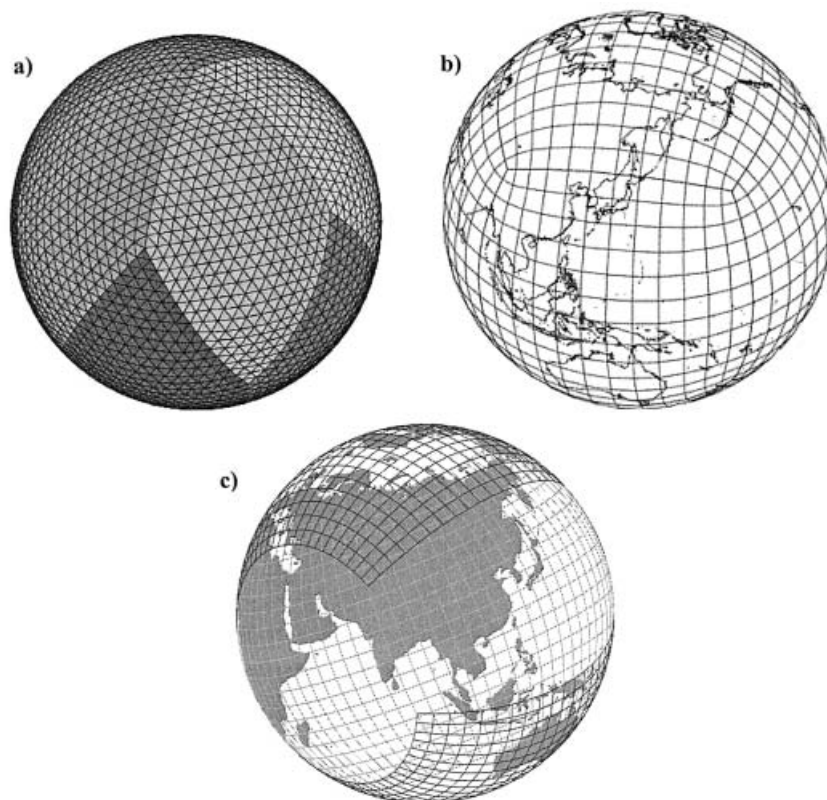


Fig. 7. **a)** Icosahedral grid. By courtesy of Masaki Satoh of FRCGC. **b)** Cubic conformal grid. By courtesy of Chiashi Muroi of JMA. **c)** Ying-Yang grid. By courtesy of Keiko Takahashi of ESC.

cubic conformal grid nonhydrostatic model (Fig. 7b). Although the uniformity of grid spacing is inferior to the icosahedral grid near the corner of each panel, this type of model has an advantage in the applicability to the regional prediction.

Some trials have been done to cover the globe by plural limited area model domains. Dudhia and Bresch (2002) developed a global version of MM5 by combining two Polar-stereographic projection domains and conducted one month simulation. A similar combined global model with MM5 has been tested at the Thai Meteorological Department with a resolution of 60–120 km (Baimoung 2006; personal communication). Takahashi et al. (2005) developed a non-hydrostatic model MSSG (Multi-Scale Simulator for Geoenvironment) on a ‘Ying-Yang’ grid system, which covers whole global surface by two rotated latitude-longitude grid domains (Fig. 7c), and performed a high resolution (5 km) global simulation on the Earth Simu-

lator. Purser et al. (2005) has also tested a Yin-Yang approach with WRF-NMM model. The interactive (2-way) nesting method is employed to exchange information between the limited-area domains in these combination-type models.

As shown in Appendix, basic equations in the curvilinear coordinate on the sphere can be converted to the latitude-longitude grid by implementing two map factors. Saito (2001) developed a global version of MRI/NPD-NHM using the cylindrical equidistant projection on the HI-VI scheme. The cylindrical equidistant projection has also been implemented to the HE-VI scheme of JMA-NHM by Yamazaki and Saito (2004). Figure 8 shows a 72 hour simulation by JMA-NHM with a horizontal resolution of 0.5 degree. In this figure, high latitude areas near north and south poles are computed two conformal polar-stereographic domains and the cylindrical equidistant projection domain covers from 70 S to 70 N. Although the computation of

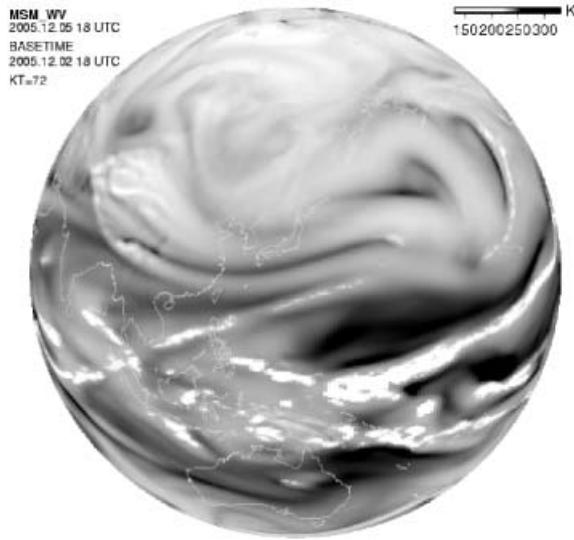


Fig. 8. Virtual water vapor satellite image by JMA nonhydrostatic model with a horizontal resolution of 0.5 degree. 72 hour forecast from the initial time 00 UTC 9 July 2002. (Yamazaki 2006; personal communication).

three domains was separately conducted in this trial, this ‘capped type’ combination model may be interesting because it can avoid the drawback of the aforementioned combined models where the joints between limited area model domains cross the mid-latitude areas over the earth.

Spectral global nonhydrostatic models have also been under development. Juang (2003) presented a HI-VI type spectral global nonhydrostatic model as a candidate of next generation NWP model at NCEP. A problem of the spherical harmonic spectral method is that the computational amount increases with third order against the size of the model domain. To overcome this problem, Yoshimura and Matsu-mura (2005) developed a global model using the double Fourier series, whose nonhydrostatic version is under development.

#### 4. The JMA nonhydrostatic model

##### 4.1 MRI-NHM

###### a. Nonhydrostatic model developed at the Forecast Research Department at MRI

Japan has long history in developing nonhydrostatic models. Takeda (1971) developed

a cloud model with seven categorized size distribution of water drops and simulated a long-lasting precipitating convective cloud. Takahashi (1975) introduced a bin method into Ogura and Phillip’s (1962) anelastic model to simulated the formation of hail with an axisymmetric model.

At MRI, Yamasaki (1975, 1984) developed a cloud model and studied interaction between cumulus convection and large-scale motion regarding the formation of tropical cyclone. Aihara and Okamura (1985) developed a nonhydrostatic compressible model and studied mountain flow. Ikawa (1988) developed a nonhydrostatic model with orography and compared three (AE, HI-VI, HE-VI) computational schemes of nonhydrostatic models. Satomura (1989) developed a fully compressible model using boundary fitting computer generated grids for simulations of small scale phenomena with steep orography. Murakami (1990) also developed an anelastic cloud model to study bulk cloud microphysics.

Ikawa’s (1988) model was initially developed as a research tool to compare the computational scheme of nonhydrostatic model with orography. Following Clark (1977), the terrain-following vertical coordinate

$$z^* = \frac{H(z - z_s)}{H - z_s}, \quad (4.1)$$

and the metric tensors for the coordinate transformations by Gal-Chen and Somerville (1975) were employed

$$\begin{aligned} G^{1/2} &= 1 - \frac{z_s}{H}, & G^{1/2}G^{13} &= \left(\frac{z^*}{H} - 1\right) \frac{\partial z_s}{\partial x}, \\ G^{1/2}G^{23} &= \left(\frac{z^*}{H} - 1\right) \frac{\partial z_s}{\partial y}, \end{aligned} \quad (4.2)$$

where  $z_s$  is the surface height and  $H$  is the model top height.

The continuity equation was given by

$$DIVT = \frac{\partial U}{\partial x} + \frac{\partial V}{\partial y} + \frac{\partial W^*}{\partial z^*} = 0, \quad (4.3)$$

for the anelastic model. Here

$$U = \bar{\rho}G^{1/2}u, \quad V = \bar{\rho}G^{1/2}v, \quad W = \bar{\rho}G^{1/2}w, \quad (4.4)$$

$$W^* = \frac{1}{G^{1/2}}(W + G^{1/2}G^{13}U + G^{1/2}G^{23}V). \quad (4.5)$$

This model was further evolved by inclusion of Lin et al. (1983) cloud microphysics, a turbulent closure model based on Deardorff (1980) and treatment surface processes for sea and land. A comprehensive documentation was published in the Technical Report of MRI (Ikawa and Saito 1991), as a nonhydrostatic model developed at the Forecast Research Department of MRI.

#### b. Nested model

The Ikawa and Saito's (1991) model was modified to a nested model (MRI-NHM) to realistically simulate mesoscale phenomena (Saito 1994). For the dynamical core, AE scheme was adopted. In order to obtain a non-divergent mass consistent initial field, a variational calculus (Sherman 1978) was implemented, where (4.3) was used as the constrain to minimize the following cost function.

$$J = \int_V \{ \alpha_1^2 (U - U_0)^2 + \alpha_1^2 (V - V_0)^2 + \alpha_2^2 (W^* - W_0^*)^2 + \lambda DIVT \} dx dy dz^*, \quad (4.6)$$

where  $U_0$ ,  $V_0$ , and  $W_0^*$  mean components of interpolated momentum (first guess) in  $x$ ,  $y$  and  $z^*$  directions, and  $\alpha_1$  and  $\alpha_2$  are weight parameters. Orlanski's (1976) radiative condition was employed with the time depending lateral boundary condition and mass fluxes through lateral boundaries were adjusted to maintain the mass conservation. Saito (1994) applied this model to reproduce a local downslope wind in Shikoku (Yamaji-kaze) and showed a good agreement between simulation and observed time evolution of surface wind when a strong typhoon approached western Japan.

#### c. Quasi-compressible version

Saito (1993) reimplemented a quasi-compressible version to MRI-NHM using the HI-VI scheme. Continuity equation was as follows

$$\frac{\partial \rho}{\partial t} + \frac{\partial U}{\partial x} + \frac{\partial V}{\partial y} + \frac{\partial W^*}{\partial z^*} = 0. \quad (4.7)$$

Pressure equation was as (1.21), and the dimension reduction method employed in AE scheme was applied to the Helmholtz-type pressure equation solver.

#### d. Fully compressible version with a map factor

A semi-implicit, fully compressible version of MRI-NHM including a map factor was developed by Saito (1997), where the linearization using the reference atmosphere was removed. Density was defined by the sum of masses of moist air and the water substances per unit volume as

$$\rho \equiv \rho_d + \rho_v + \rho_c + \rho_r + \rho_i + \rho_s + \rho_g, \quad (4.8)$$

where subscripts  $c$ ,  $r$ ,  $i$ ,  $s$  and  $g$  stand for the cloud water, rain, cloud ice, snow, and graupel, respectively.  $\rho_d$  is the density of dry air and  $\rho_v$  that of water vapor.

Introducing a map factor  $m$ , the continuity equation is given by

$$G^{1/2} \frac{\partial \rho}{\partial t} + DIVT = PRC, \quad (4.9)$$

where  $DIVT$  is the total divergence in  $z^*$  coordinate and  $U$ ,  $V$ , and  $W^*$  are defined by

$$DIVT = m^2 \left( \frac{\partial U}{\partial x} + \frac{\partial V}{\partial y} \right) + m \frac{\partial W^*}{\partial z^*}, \quad (4.10)$$

$$U = \frac{\rho G^{1/2} u}{m}, \quad V = \frac{\rho G^{1/2} v}{m}, \quad W = \frac{\rho G^{1/2} w}{m}, \quad (4.11)$$

$$W^* = \frac{1}{G^{1/2}} \{ W + m(G^{1/2} G^{13} U + G^{1/2} G^{23} V) \}. \quad (4.12)$$

$PRC$  in (4.9) is the fall-out of water substances written in  $z^*$  coordinate:

$$PRC = \frac{\partial}{\partial z^*} (\rho_a V_r q_r + \rho_a V_s q_s + \rho_a V_g q_g), \quad (4.13)$$

where  $\rho_a$  is the density of moist air and  $V$  the terminal velocity of precipitable water substances (rain, snow and graupel). The state equation is given as the diagnostic equation for density as

$$\rho = \frac{p_0}{R \theta_m} \left( \frac{p}{p_0} \right)^{C_v/C_p}, \quad (4.14)$$

where  $\theta_m$  is the mass-virtual potential temperature defined by

$$\theta_m = \theta (1 + 0.608 q_v) \times (1 - q_c - q_r - q_i - q_s - q_g). \quad (4.15)$$

The buoyancy term is defined by

$$BUOY = \sigma \frac{\rho G^{1/2} \theta'_m g}{\theta_m} - (1 - \sigma)(\rho - \bar{\rho})gG^{1/2}, \quad (4.16)$$

where  $\sigma$  is a switching parameter, and  $\sigma = 0$  is used for the direct computation of the buoyancy from the density perturbation. The pressure equation is obtained from (4.9) and (4.14) as

$$\frac{\partial P}{\partial t} = C_m^2 (PFT - DIVT + PRC), \quad (4.17)$$

where  $C_m$  is given by

$$C_m^2 = \frac{C_p}{C_v} R \theta_m \left( \frac{p}{p_0} \right)^{R/C_p}, \quad (4.18)$$

and  $PFT$  is the local time tendency of the mass-virtual potential temperature,

$$PFT = \frac{\rho G^{1/2}}{\theta_m} \frac{\partial \theta_m}{\partial t}. \quad (4.19)$$

Another important modification of the model which contributed to improve model's performance was implementation of the modified centered difference advection scheme (Kato 1998). This scheme is a flux limiter-type flux correction scheme, which removes numerical errors due to the finite difference approximation and assure the monotonicity (Fig. 9).

In the cloud physics, to assure the computational stability for sedimentation of rain, the box Lagrangian scheme (Kato 1995) was implemented. Furthermore atmospheric radiation schemes were also incorporated into the model. These modifications extended MRI-NHM to a full-scale mesoscale model, which was used for several studies at MRI including international cooperative programs; e.g., Fujibe et al. (1999) for the Southern Alps Experiment (SALPEX) in New Zealand and Saito et al. (2001a) for the Maritime Continent Thunderstorm Experiment (MCTEX) in Australia.

#### e. MRI/NPD-NHM

In 1999, a cooperative effort to develop a community model for NWP and research started between the Numerical Prediction Division (NPD) of JMA and MRI. As the first step, the HE-VI scheme was reimplemented into MRI-NHM by Muroi et al. (1999), considering the

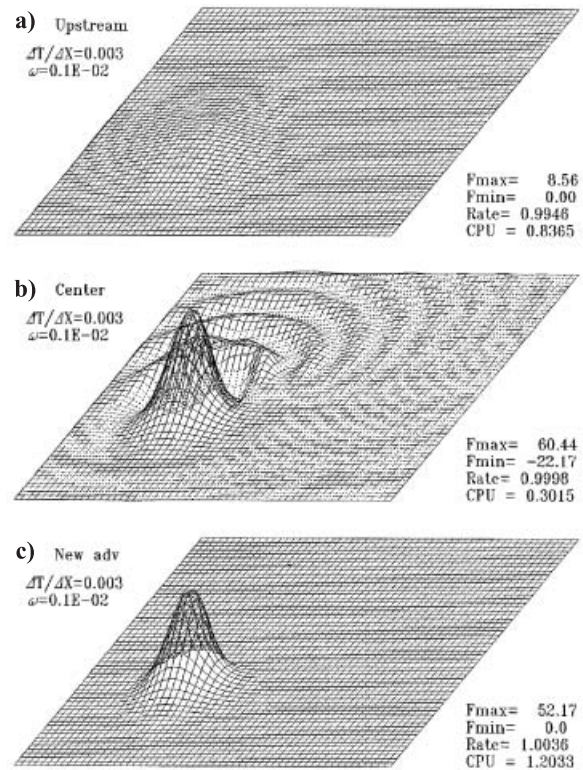


Fig. 9. Effect of the flux correction scheme by Kato (1998) employed in MRI-NHM. Results of 1000 time step integration of a perturbation with 2-D Gaussian function. **a)** First order upstream scheme. **b)** Second order centered scheme. **c)** Second order centered scheme with the flux correction scheme. After Saito and Kato (1999).

computational efficiency in the parallel computing architecture. In collaboration with RIST, code parallelization of the model to handle the distributed memory parallel computers was done. A unified model, “MRI/NPD-NHM,” was completed and a comprehensive description was published in the Technical Report of MRI (Saito et al. 2001b).

#### 4.2 Operational application of JMA-NHM

##### a. 10 km nonhydrostatic MSM

Since 2001, development of an operational nonhydrostatic mesoscale model (nonhydrostatic MSM) has been made at NPD collaborating with MRI. In addition to the three conformal projections, the cylindrical equidistant projection was implemented as the optional

choice (see Appendix). The total divergence and  $U$ ,  $V$ , and  $W^*$  are defined by

$$DIVT = m_1 m_2 \left( \frac{\partial U}{\partial x} + \frac{\partial V}{\partial y} \right) + m_3 \frac{\partial W^*}{\partial z^*}, \quad (4.20)$$

and

$$U = \frac{\rho G^{1/2} u}{m_2}, \quad V = \frac{\rho G^{1/2} v}{m_1}, \quad W = \frac{\rho G^{1/2} w}{m_3}, \quad (4.21)$$

$$W^* = \frac{1}{G^{1/2}} \left\{ W + \frac{m_1 m_2}{m_3} (G^{1/2} G^{13} U + G^{1/2} G^{23} V) \right\}. \quad (4.22)$$

The continuity equation is

$$G^{1/2} \frac{\partial \rho}{\partial t} + DIVT = PRC + \rho DIF.q_v, \quad (4.23)$$

where the second term in *r.h.s.* of (4.23) is the diffusion of water vapor in unit time, which includes sub-grid scale turbulent mixing and computational diffusion. This term was implemented by Saito (2004) to consider the surface evaporation of water vapor, which offsets the loss of mass by precipitation in total mass conservation.

Several modifications were added to enhance the computational efficiency, robustness and accuracy as an operational NWP model. Higher order (third to fifth) advection schemes which consider staggered grid configuration were implemented by Fujita (2003). In the operational forecasting at JMA, the fourth-order scheme is chosen, considering computational cost and matching with the advection correction scheme.

A time splitting scheme of gravity waves and advection terms was implemented by Saito (2003a). In the new splitting scheme, higher-order advection terms with the flux correction scheme are fully evaluated at the center of the leapfrog time step, and then the lower-order (second-order) components at each short time step are adjusted in the latter half of the leapfrog time integration. This scheme is different from the Hsu and Sun's (2001) time splitting scheme of advection where the time splitting of advection is discussed in a forward base two time level model.

In order to attenuate computational instability of sound waves in the HE-VI time integration scheme, an acoustic filter was introduced.

Although the idea is based on Skamarock and Klemp (1992), the damping terms act on the flux form total divergence (*DIVT*). An option of 2-dimensional decomposition for parallel computing was implemented where a special node can be exclusively spared for the output process on user's demand (Aranami and Ishida 2005).

As for physical processes, the Kain-Fritsch convective parameterization scheme (K-F scheme; Kain and Fritsch 1993) was implemented with a modification by Yamada (2003). Several points have been revised by Ohmori and Yamada (2004) to improve its performance with a 10 km resolution for prediction of heavy rainfall events in Japan, where moist and unstable maritime air-mass prevails in summer. In order to control the grid point storms and the associated intense grid scale precipitation, the targeted moisture diffusion (TMD) has been implemented (Saito and Ishida 2005), where an artificial second order horizontal diffusion is applied to water vapor when strong upward motions exist.

In order to ameliorate cold and wet biases at the surface, the value of scalar roughness lengths for heat and moisture were reduced to about 1/7.4 of momentum roughness length following Garratt and Francey (1978). Furthermore, computation of bulk coefficients for surface fluxes over land was changed from Sommeria (1976) to Louis et al. (1982), with implementation of a stomatal resistance to express the diurnal and seasonal changes of the evapotranspiration at surface.

As for boundary layer processes, the vertical mixing length in the TKE equation was computed by the PBL height following Sun and Chang (1986) to consider the non-local effect. Furthermore, a diagnostic TKE scheme was implemented to prevent computational mode, where a local equilibrium between the buoyancy, shear production terms and viscosity dissipation term was assumed (Kumagai 2004a, 2004b). Implicit treatment of vertical diffusion was implemented where surface flux is computed fully implicitly using bulk coefficients.

On 1 September 2004, after five months pre-operational runs, JMA replaced the former hydrostatic mesoscale model ('hydrostatic MSM') with the JMA-NHM ('nonhydrostatic MSM'). Eighteen-hour forecasts were run 4 times a

day to support disaster prevention and the very short range forecast of precipitation at JMA. A domain of  $3600 \text{ km} \times 2880 \text{ km}$  which covers Japan and its surrounding areas (Fig. 3) was taken. Vertically, 40 levels with variable grid intervals of  $\Delta z = 40 \text{ m}$  to  $1180 \text{ m}$  were employed, where the model top and the lowest level are located at  $22060 \text{ m}$  and  $20 \text{ m}$ , respectively.

Initial conditions of horizontal wind, temperature, water vapor, and surface pressure were given by the JMA Meso 4D-Var (Koizumi et al. 2005) analysis 6 hourly as in the former hydrostatic MSM. Initial conditions of cloud microphysical quantities were given by the 6-hour forecast cycle. Lateral boundary conditions were supplied from forecasts of the  $20 \text{ km}$  resolution Regional Spectral Model of JMA (RSM), while the initial times of RSM were 6 or 12 hours earlier than MSM as in the operational condition.

Detail of the  $10 \text{ km}$  nonhydrostatic MSM is given in Saito et al. (2006).

#### b. High resolution (5 km) MSM

Since March 2006, horizontal and vertical resolutions of nonhydrostatic MSM have been enhanced from  $10 \text{ km}$  L40 to  $5 \text{ km}$  L50 (Ishida et al. 2005). The model operation has also been increased from 4 times a day (6 hourly) to 8 times (3 hourly), to provide more frequent forecasts. Time step for leap-frog integration has been changed from  $40 \text{ sec}$  to  $24 \text{ sec}$ .

Some modifications have been added to physical processes. In the atmospheric radiation scheme of the  $10 \text{ km}$  MSM, cloud was assumed as a black body and cloud optical properties were given by empirical constants both in the hydrostatic and nonhydrostatic models. In the new radiation scheme (Nagasawa and Kitagawa 2005) cloud optical properties are determined by cloud water/ice contents and their effective radius. This modification reduces the negative bias of  $200 \text{ hPa}$  temperature and improves the prediction of diurnal change of the surface temperature.

The convective parameterization is still required at  $5 \text{ km}$ , because without convective parameterization the model overestimates intense rain more than  $20 \text{ mm/hour}$  and underestimates weak to moderate rains less than several  $\text{mm/hour}$ . In K-F scheme, following points have been revised (Ohmori and Yamada

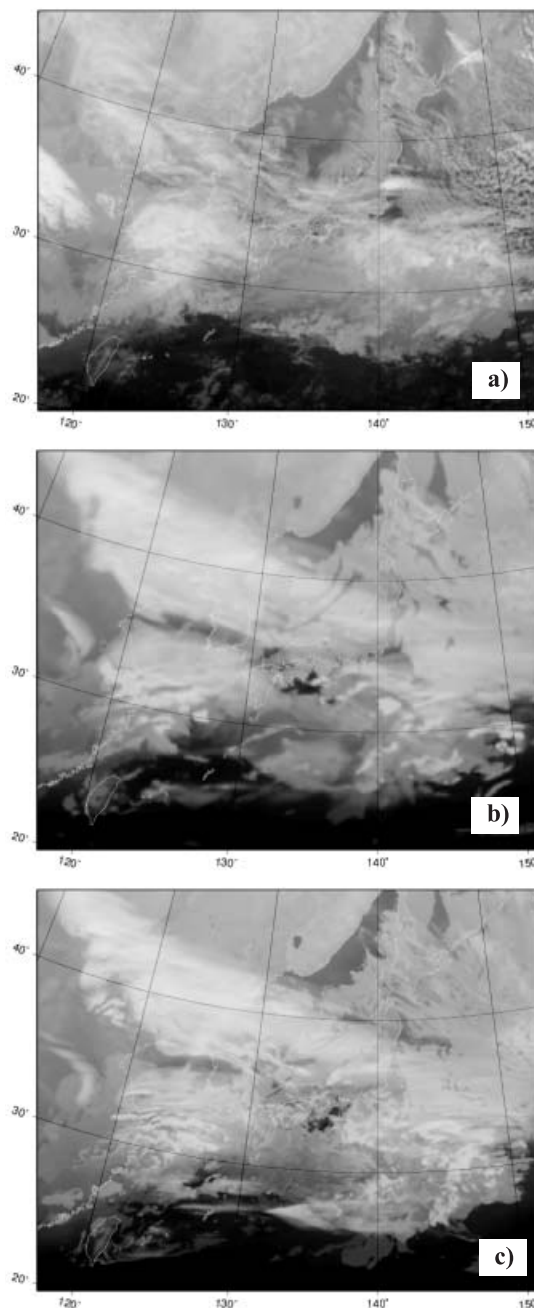


Fig. 10. **a)** Infrared image by MTSAT-1 at 00 UTC, 20 January 2006. **b)** Corresponding forecast by  $10 \text{ km}$  MSM. Initial time is 18 UTC, 19 January 2006. **c)** Same as in b) but  $5 \text{ km}$  MSM.

2006); 1) conversion from convective condensate to rain is reduced, 2) time scales of deep and shallow convection are reduced, and 3) threshold values for conversion from cloud

water/ice to precipitation are increased. These modifications contribute to improve both bias and threat scores. Threshold value to invoke the targeted moisture diffusion has been also changed from 2 m/s to 3 m/s.

In the TKE scheme, the value of coefficient to compute eddy viscosity has been decreased above the boundary layer. Same mixing length is used both in the horizontal and the vertical directions.

Figures 10b and 10c show virtual infrared satellite images with the 10 km and 5 km non-hydrostatic MSMs. Although these two figures resemble each other, the predicted image with the 5 km MSM (Fig. 10c) is more similar to the observation (Fig. 10a) by the virtue of the higher resolution. Characteristics of low level

clouds over the sea off the east coast of Japan, upper clouds west of Japan, and convective clouds over the Pacific Ocean are well simulated in the 5 km MSM.

Figure 11 shows QPF performance of MSM. In this figure, scores for moderate to intense rain with a threshold value of 10 mm for 3 hours at FT = 6–9 are indicated. This forecast time is important for the operational very short range forecast of precipitation at JMA. Given the verification grid size of 10 km, this validation is a very tough condition for a NWP model, thus values of threat scores are not so high. After the commencement of operational run of the hydrostatic MSM in March 2001, several modifications shown in Table 5 have been implemented in MSM.

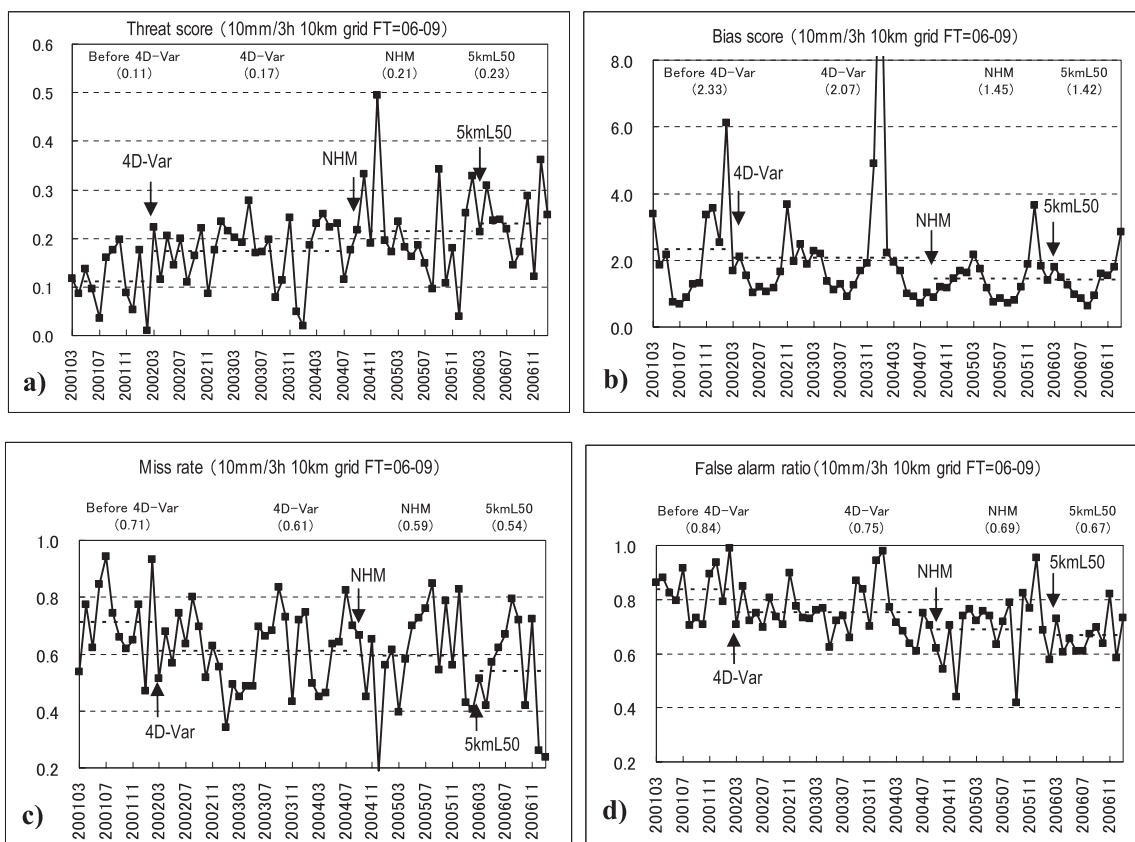


Fig. 11. Performance of MSM from March 2001 to January 2007. Verification grid is 10 km. **a)** Threat score for 3 hour precipitation at FT = 9 with a threshold value of 10 mm/3 hour. **b)** Same as in a) but bias score. **c)** Same as in a) but miss rate. **d)** Same as in a) but false alarm ratio.

Table 5. Main operational changes in the JMA mesoscale model.

Mar. 2001	Start of Mesoscale NWP
Jun. 2001	Wind profiler data
Mar. 2002	4D-Var in MSM
Aug. 2002	Domestic ACARS data
Oct. 2003	SSM/I precipitable amount
Jul. 2004	QuikSCAT Seawinds
Sep. 2004	Nonhydrostatic model
Mar. 2005	Doppler radar radial winds
Mar. 2006	5 km L50, 3 hourly

Figure 11a shows the threat score. The averaged score before implementation of Meso 4D-Var in March 2002 was 0.11, but after March 2006, enhancement of horizontal and vertical resolutions, the score has been improved to 0.23. The bias score (Fig. 11b) had shown a tendency of overestimation of precipitation in winter, but after the implementation of the nonhydrostatic model in September 2004, this overestimation has been ameliorated. This is mainly attained by the inclusion of cloud microphysics in the nonhydrostatic MSM, because the hydrostatic MSM regarded the condensate as the surface precipitation. The miss rate (Fig. 11c) was decreased from 0.71 to 0.61 by implementation of 4D-Var, and decreased to 0.54 in the 5 km MSM. The false alarm ratio (Fig. 11d) has been decreased from 0.84 before March 2002 to 0.67 after March 2006. This means that recent improvement of threat scores in MSM has been attained by decrease of both the miss rate and the false alarm ratio. To decrease both values less than 0.5 may be a target of the JMA short range QPF in the near future.

### c. Recent developments and plans in near future

In May 2007, JMA will extend the forecast time of MSM from 15 hours to 33 hours at the initial times of 03, 09, 15 and 21 UTC. These extended forecasts will cover information for disaster prevention up to 24 hours (Hara et al. 2007).

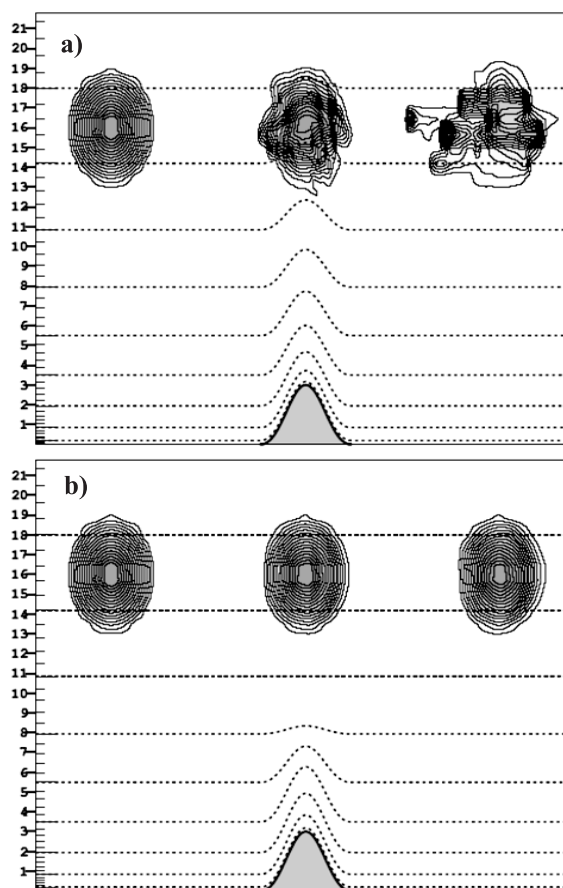


Fig. 12. Result of the idealized advection experiment. Contour interval is  $5.0 \times 10^{-10}$  Kg/Kg. Fourth order advection with the flux correction scheme is used. **a)** Water vapor at FT = 0, 12 and 24 with  $z^*$  coordinate. **b)** Same as in a) but with the hybrid coordinate. After Ishida (2007).

As the modification of dynamics, a generalized hybrid vertical coordinate

$$\zeta = z - z_s f(\zeta), \quad (4.24)$$

will be introduced, which approaches the  $z^*$  coordinate near surface and the  $z$  coordinate near model top (Ishida 2007). Here  $f(0) = 1$ ,  $f(H) = 0$  and  $f(\zeta)$  is determined so that  $\partial z / \partial \zeta$  is positive and the second derivative of  $f(\zeta)$  is differentiable. Figure 12 shows a result of a comparative experiment of idealized advection with  $z^*$  and the generalized hybrid vertical

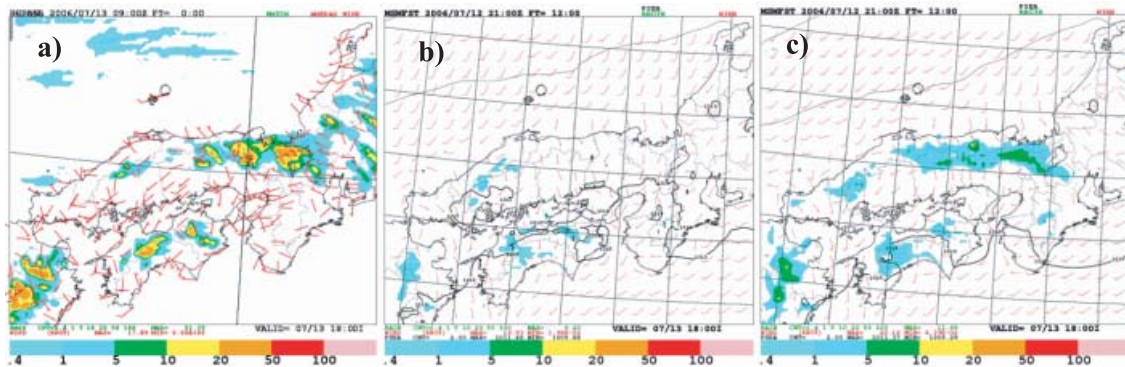


Fig. 13. Three hour precipitation at 09 UTC 13 July 2006. **a)** Observed Radar-AMeDAS rain. **b)** Predicted rain with the operational K-F scheme at FT = 12 (Initial time is 21 UTC 12 July 2006). **c)** Same as in b) but with the Modified K-F scheme using the water vapor trigger function.

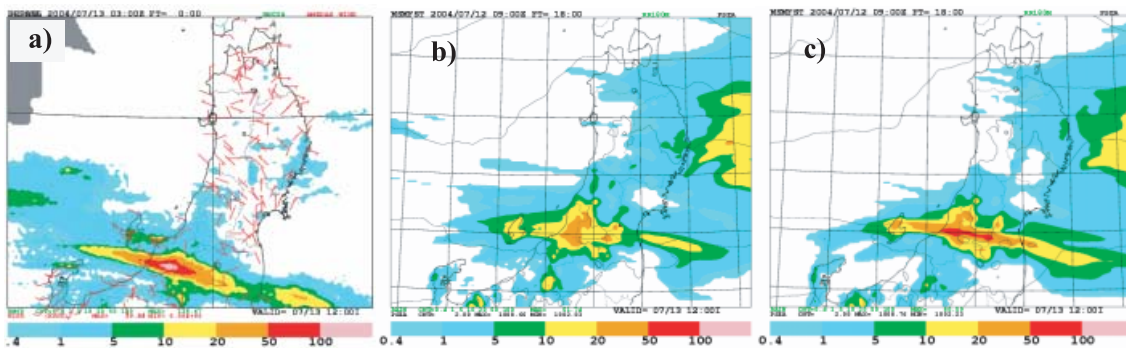


Fig. 14. Three hour precipitation at 03 UTC 13 July 2004. **a)** Observed Radar-AMeDAS rain. **b)** Predicted rain with the original MSM at FT = 18 (Initial time is 09 UTC 12 July 2004). **c)** Same as in b) but with the MY3 closure model and the modified radiation scheme using the partial condensation for cloudiness. After Hara (2007).

coordinates<sup>7</sup>. In this experiment, a mountain whose height is 3000 m is located at the model domain, and water vapor is advected by horizontal wind of  $u = 2.5$  m/s. In the  $z^*$  coordinate (Fig. 12a), the shape of water vapor is distorted when the water vapor mass passes above the mountain, while in the hybrid coordinates (Fig. 12b), the original shape is well preserved until FT = 24 hours.

In the cloud microphysics, fall-out of cloud ice is newly considered in addition to the former precipitable quantities (rain, snow and graupel) to prevent an excessive accumulation of cloud

ice in the upper model atmosphere. In K-F scheme for convection, perturbation depending on relative humidity is added in the trigger function to reduce the overestimation of convective rain induced by orography. This modification also improves the model's performance to simulate the diurnal change of convection. Figure 13 shows an example of the prediction with the original and modified K-F schemes. Observed diurnal convective rains over the inland of the western part of Japan are well simulated by the model with the modified K-F scheme.

As for the turbulent model, a Mellor and Yamada level 3 closure model (MY3; Nakanishi and Niino 2004, 2006) will be first implemented as the operational NWP model to reduce model

<sup>7</sup> Similar idealized experiment for hybrid coordinate is given in Schär et al. (2002).

Table 6. Specifications of JMA mesoscale model (nonhydrostatic MSM).

	As of September 2004 (Saito et al. 2006)	As of March 2006	End of 2007
Horizontal mesh (resolution)	361 × 289 (10 km)	721 × 577 (5 km)	No change
Mapping	Lambert conformal	No change	
Levels	40 terrain-following	50 terrain-following	50 generalized hybrid
Model top	22060 m	21800 m	No change
Horizontal discretization	Arakawa C	No change	
Horizontal advection	Flux form 4th order with advection correction and time splitting		
Gravity waves	Time splitting		
Sound waves	HE-VI		
Forecast period	18 hours		15 hours
Initial time	00, 06, 12, 18 UTC	00, 03, 06, 09, 12, 15, 18, 21 UTC	
Initial conditions	Meso 4D-Var (hydrostatic)	No change	JNoVA 4D-Var (nonhydrostatic)
Lateral boundary	RSM (20 km L40) 12 hourly		GSM (TL959 L60) 6 hourly
Prognostic variables	$U, V, W, P, \theta, q_v, q_c, q_i,$ $q_r, q_s, q_g$		$U, V, W, P, \theta, q_v, q_c, q_i, q_r, q_s,$ $q_g, TKE, \theta_l'^2, q_w'^2, \theta_l'q_w'$
Moist physics	3 ice bulk microphysics	3 ice bulk microphysics (parameters revised)	3 ice bulk microphysics with fall-out of cloud ice
Convection	Kain-Fritsch scheme	Kain-Fritsch scheme (parameters revised)	Kain-Fritsch scheme with water vapor trigger function
Turbulence	diagnostic TKE scheme	No change	Mellor Yamada Level 3
Radiation	cloud optical properties with empirical constants	cloud optical properties with diagnosed cloud water/ice contents and effective radius	detailed long wave radiation scheme for clear sky partial condensation by PDF in the MY3 closure model for cloudiness

errors in boundary layer. In addition to the prognostic turbulent kinetic energy ( $TKE$ ), fluctuations of liquid water potential temperature ( $\theta_l'^2$ ) and total water content ( $q_w'^2$ ) and their correlation ( $\theta_l'q_w'$ ) are treated as the prognostic variables. The effect of counter-gradient diffusion is naturally considered in the computation of the diffusion coefficients without a non-local parameterization. In the radiation scheme, the

long wave radiation scheme for clear sky employed in the operational JMA global model will be implemented to reduce the negative temperature bias in the lower atmosphere. To evaluate the degree of cloudiness, the partial condensation computed by the probability density function in the MY3 closure model is considered. Figure 14 shows an example of the prediction with the original and modified models.

Observed line-shaped precipitation over the northern part of central Japan is well simulated by the modified MSM with the MY3 closure model and the new radiation scheme.

JMA is planning to introduce a very high resolution (20 km) semi-Lagrangian global spectral model (GSM) in late 2007. Since the high resolution global model will be run 6 hourly, it will supply the boundary conditions to MSM more frequently. A nonhydrostatic 4D-Var data assimilation system (JNoVA; JMA Nonhydrostatic model based Variational data assimilation system; Honda et al. 2005) is planned to be operational in late 2007 to supply the 5 km MSM more accurate initial conditions. Horizontal resolution of the 4D-Var inner loop will be enhanced from 20 km of Meso 4D-Var to 10 km in JNoVA, while a cloud resolving 4D-var system is under development at MRI (Kawabata et al. 2006). Expected specifications of MSM up to the end of 2007 is listed in Table 6. Assimilation of GPS data will start within a few years to improve the analysis of water vapor.

JMA is planning to implement a mesoscale ensemble prediction system (MEPS) in the next NWP system. Developments of MEPS have been underway with various approaches including downscaling of global EPS, BGM and SV methods. A preliminary trial of MEPS for Japan area is seen in Seko et al. (2007). A local ensemble Kalman filter technique using JMA-NHM has also been developed (Miyoshi and Aranami 2006).

Development of a high resolution JMA-NHM has been underway at MRI and NPD for next generation cloud resolving NWP. Test of a 2 km resolution local NWP model for the very short range forecast of precipitation will be started at NPD in May 2007.

### Acknowledgements

Some parts of this paper originate from the first author's Japanese reviews appeared in Saito (1999) and Saito (2003b). The authors thank Chiashi Muori of NPD, and Teruyuki Kato and Hisaki Eito of MRI for their help and courtesy for quotation of figures. The latest version of the JMA nonhydrostatic model has been developed at NPD collaborating with MRI. Thanks are extended to Ryoji Nagasawa, Hi-

roshi Nakayama, Mitsuo Ohizumi, Shugo Hayashi and other staff members of NPD and MRI.

The authors also thank Brian Golding, Andrew Lorenc and Terry Davies of UKMO, Juergen Steppeler and Detlev Majewski of DWD, Jean Cote and Martin Charron of RPN, Zavis Janjic, Geoff DiMego and Henry Juang of NCEP, Joseph Klemp and Jimmy Dudhia of NCAR, Dehui Chen of CAMS/CMA, Michel Deque and Francois Bouttier of Meteo France, William Cotton of CSU, Ping-wah Li, Edwin Lai and Wai-kin Wong of HKO, Masaki Satoh of FRCGC and Keiko Takahashi of the Earth Simulator Center for their valuable information and figures. We appreciate helpful comments of the two anonymous reviewers which contributed to improve the original manuscript.

## Appendix

### Basic equations on orthogonal coordinate on the sphere

Basic equations on the Cartesian coordinate can be expanded to the equations in the orthogonal coordinate on the sphere. Consider an orthogonal coordinate on the sphere (Fig. A1). Let tangential unit vectors in  $\zeta$ -axis and  $\eta$ -axis  $\mathbf{i}$  and  $\mathbf{j}$ , respectively, and take a unit vector  $\mathbf{k}$  in the vertical direction, where  $z$ -axis is linear coordinate. In the orthogonal coordinate, inner products of each vectors are zero.

The distance on the projection axis ( $ds_1, ds_2, ds_3$ ) between two points  $P(\zeta, \eta, z)$  and  $Q(\zeta + d\zeta, \eta + d\eta, z + dz)$  can be given by

$$ds_1 = \frac{d\zeta}{m}, \quad ds_2 = \frac{d\eta}{n}, \quad ds_3 = dz, \quad (\text{A.1})$$

where  $m$  and  $n$  is the map factor.

Component of velocity vector in each axis ( $u, v, w$ ) is given by

$$\mathbf{V} = \mathbf{i}u + \mathbf{j}v + \mathbf{k}w, \quad (\text{A.2})$$

$$u = \frac{ds_1}{dt} = \frac{1}{m} \frac{d\zeta}{dt}, \quad v = \frac{ds_2}{dt} = \frac{1}{n} \frac{d\eta}{dt},$$

$$w = \frac{ds_3}{dt} = \frac{dz}{dt}. \quad (\text{A.3})$$

Momentum equation with rotation of Earth is

$$\frac{d\mathbf{V}}{dt} = -2\boldsymbol{\Omega} \times \mathbf{V} - \frac{1}{\rho} \nabla p + \mathbf{k}g \quad (\text{A.4})$$

where

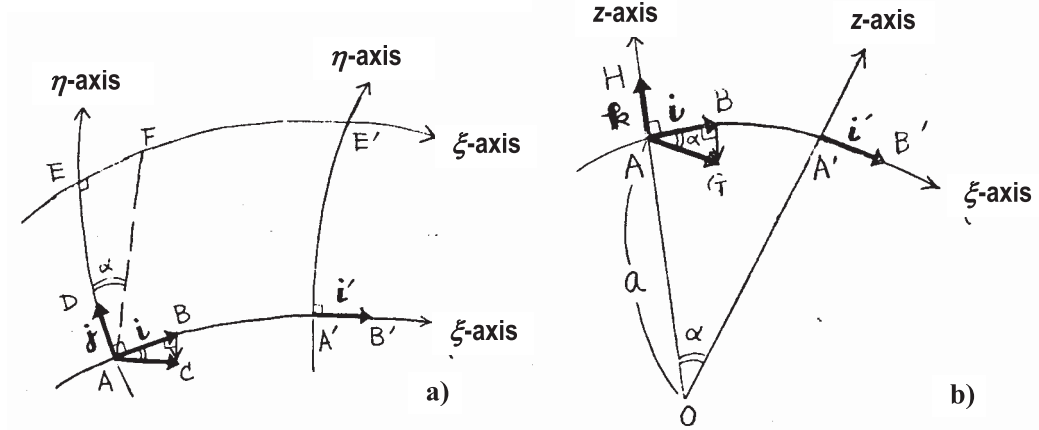


Fig. A1. a) Orthogonal curvilinear coordinate at a plain of  $z = \text{constant}$ . b) Cross-section of  $\xi$ - $z$  plain. Reproduced from Kikuchi (1975).

$$\nabla = \mathbf{i}m \frac{\partial}{\partial \xi} + \mathbf{j}n \frac{\partial}{\partial \eta} + \mathbf{k} \frac{\partial}{\partial z}, \quad (\text{A.5})$$

$$\frac{d}{dt} = \frac{\partial}{\partial t} + mu \frac{\partial}{\partial \xi} + nv \frac{\partial}{\partial \eta} + w \frac{\partial}{\partial z}, \quad (\text{A.6})$$

and  $\Omega$  is angular velocity vector of earth's rotation. From above equations, we obtain

$$\begin{aligned} \frac{d\mathbf{V}}{dt} &= \mathbf{i} \frac{du}{dt} + \mathbf{j} \frac{dv}{dt} + \mathbf{k} \frac{dw}{dt} + u \frac{d\mathbf{i}}{dt} + v \frac{d\mathbf{j}}{dt} + w \frac{d\mathbf{k}}{dt} \\ &= \mathbf{i} \frac{du}{dt} + \mathbf{j} \frac{dv}{dt} + \mathbf{k} \frac{dw}{dt} + u \left( mu \frac{\partial \mathbf{i}}{\partial \xi} + nv \frac{\partial \mathbf{i}}{\partial \eta} \right) \\ &\quad + v \left( mu \frac{\partial \mathbf{j}}{\partial \xi} + nv \frac{\partial \mathbf{j}}{\partial \eta} \right) \\ &\quad + w \left( mu \frac{\partial \mathbf{k}}{\partial \xi} + nv \frac{\partial \mathbf{k}}{\partial \eta} \right). \end{aligned} \quad (\text{A.7})$$

Local derivative of each unit vector along the each axis is

$$\begin{aligned} \frac{\partial \mathbf{i}}{\partial \xi} &= -\mathbf{j}n \frac{\partial}{\partial \eta} \left( \frac{1}{m} \right) - \mathbf{k} \frac{1}{am}, & \frac{\partial \mathbf{i}}{\partial \eta} &= \mathbf{j}m \frac{\partial}{\partial \xi} \left( \frac{1}{n} \right), \\ \frac{\partial \mathbf{j}}{\partial \xi} &= \mathbf{i}n \frac{\partial}{\partial \eta} \left( \frac{1}{m} \right), & \frac{\partial \mathbf{j}}{\partial \eta} &= -\mathbf{i}m \frac{\partial}{\partial \xi} \left( \frac{1}{n} \right) - \mathbf{k} \frac{1}{an}, \\ \frac{\partial \mathbf{k}}{\partial \xi} &= -\mathbf{i} \frac{1}{am}, & \frac{\partial \mathbf{k}}{\partial \eta} &= -\mathbf{j} \frac{1}{an}, \end{aligned} \quad (\text{A.8})$$

where  $a$  is the radius of the Earth. Using above, the curvilinear term, the last three terms in *r.h.s.* of (A.7) becomes

$$\begin{aligned} \mathbf{M} &= u \left( mu \frac{\partial \mathbf{i}}{\partial \xi} + nv \frac{\partial \mathbf{i}}{\partial \eta} \right) + v \left( mu \frac{\partial \mathbf{j}}{\partial \xi} + nv \frac{\partial \mathbf{j}}{\partial \eta} \right) \\ &\quad + w \left( mu \frac{\partial \mathbf{k}}{\partial \xi} + nv \frac{\partial \mathbf{k}}{\partial \eta} \right) \\ &= \mathbf{i}mnv \left\{ u \frac{\partial}{\partial \eta} \left( \frac{1}{m} \right) - v \frac{\partial}{\partial \xi} \left( \frac{1}{n} \right) \right\} \\ &\quad + \mathbf{i} \frac{wu}{a} + \mathbf{j}mnu \left\{ -u \frac{\partial}{\partial \eta} \left( \frac{1}{m} \right) + v \frac{\partial}{\partial \xi} \left( \frac{1}{n} \right) \right\} \\ &\quad + \mathbf{j} \frac{wv}{a} - \mathbf{k} \frac{u^2 + v^2}{a}. \end{aligned} \quad (\text{A.9})$$

Continuity equation is

$$\begin{aligned} \frac{d\rho}{dt} + \rho(\nabla \cdot \mathbf{V}) &= 0, \\ \nabla \cdot \mathbf{V} &= \left( \mathbf{i}m \frac{\partial}{\partial \xi} + \mathbf{j}n \frac{\partial}{\partial \eta} + \mathbf{k} \frac{\partial}{\partial z} \right) (\mathbf{i}u + \mathbf{j}v + \mathbf{k}w) \\ &= m \frac{\partial u}{\partial \xi} + \mathbf{i}m \left( v \frac{\partial \mathbf{j}}{\partial \xi} + w \frac{\partial \mathbf{k}}{\partial \xi} \right) \\ &\quad + n \frac{\partial v}{\partial \eta} + \mathbf{j}n \left( u \frac{\partial \mathbf{i}}{\partial \eta} + w \frac{\partial \mathbf{k}}{\partial \eta} \right) + \frac{\partial w}{\partial z} \\ &= m \frac{\partial u}{\partial \xi} + mnv \frac{\partial}{\partial \eta} \left( \frac{1}{m} \right) + \frac{w}{a} + n \frac{\partial v}{\partial \eta} \\ &\quad + mnu \frac{\partial}{\partial \xi} \left( \frac{1}{n} \right) + \frac{w}{a} + \frac{\partial w}{\partial z} \\ &= mn \left\{ \frac{\partial}{\partial \xi} \left( \frac{u}{n} \right) + \frac{\partial}{\partial \eta} \left( \frac{v}{m} \right) \right\} \\ &\quad + \frac{\partial w}{\partial z} + \frac{2w}{a}. \end{aligned} \quad (\text{A.10})$$

If we rewrite  $(\xi, \eta)$  to  $(x, y)$  as in the conventional form, (A.4) can be written as

$$\frac{du}{dt} = Cor_1 + Crv_1 - \frac{1}{\rho} m \frac{\partial p}{\partial x}, \quad (\text{A.11})$$

$$\frac{dv}{dt} = Cor_2 + Crv_2 - \frac{1}{\rho} n \frac{\partial p}{\partial y}, \quad (\text{A.12})$$

$$\frac{dw}{dt} = Cor_3 + Crv_3 - \frac{1}{\rho} \frac{\partial p}{\partial z} - g, \quad (\text{A.13})$$

where *Cor* and *Crv* are Coriolis and curvature terms and expressed as follows

$$Cor_1 = 2\Omega \sin \varphi v - 2\Omega \cos \varphi \cos \Delta\lambda w, \quad (\text{A.14})$$

$$Cor_2 = -2\Omega \cos \varphi \sin \Delta\lambda w - 2\Omega \sin \varphi u, \quad (\text{A.15})$$

$$Cor_3 = 2\Omega \cos \varphi \cos \Delta\lambda u + 2\Omega \cos \varphi \sin \Delta\lambda v, \quad (\text{A.16})$$

$$Crv_1 = mnv \left\{ v \frac{\partial}{\partial x} \left( \frac{1}{n} \right) - u \frac{\partial}{\partial y} \left( \frac{1}{m} \right) \right\} - \frac{uw}{a}, \quad (\text{A.17})$$

$$Crv_2 = -mnu \left\{ v \frac{\partial}{\partial x} \left( \frac{1}{n} \right) - u \frac{\partial}{\partial y} \left( \frac{1}{m} \right) \right\} - \frac{vw}{a}, \quad (\text{A.18})$$

$$Crv_3 = \frac{u^2 + v^2}{a}. \quad (\text{A.19})$$

Note that in the longitude latitudinal grid, if we take  $(x, y)$  to  $(\lambda, \varphi)$ , and let

$$m = \frac{1}{a \cos \varphi}, \quad n = \frac{1}{a}, \quad (\text{A.20})$$

$$u = a \cos \varphi \frac{d\lambda}{dt}, \quad v = a \frac{d\varphi}{dt}, \quad (\text{A.21})$$

then (A.11)–(A.13) with (A.17)–(A.19) are reduced to the well-known conventional equations in the spherical coordinate

$$\begin{aligned} \frac{du}{dt} - \frac{uv \tan \varphi}{a} + \frac{uw}{a} + \frac{1}{\rho a \cos \varphi} \frac{\partial p}{\partial \lambda} \\ = 2\Omega v \sin \varphi - 2\Omega w \cos \varphi, \end{aligned} \quad (\text{A.22})$$

$$\frac{dv}{dt} + \frac{u^2 \tan \varphi}{a} + \frac{vw}{a} + \frac{1}{\rho a} \frac{\partial p}{\partial \varphi} = -2\Omega u \sin \varphi, \quad (\text{A.23})$$

$$\frac{dw}{dt} - \frac{u^2 + v^2}{a} + \frac{1}{\rho} \frac{\partial p}{\partial z} + g = 2\Omega u \cos \varphi. \quad (\text{A.24})$$

In JMA-NHM, in addition to the conformal pro-

jection where  $m$  is set to equal to  $n$ , the cylindrical equidistant projection is available by setting two map factors as

$$m = \frac{\cos \varphi_0}{\cos \varphi}, \quad n = 1, \quad (\text{A.25})$$

where  $\varphi_0$  is the standard latitude.

## References

- Ajmani, K., W. Ng, and M. Liou, 1994: Preconditioned Conjugate Gradient Methods for the Navier-Stokes Equations. *J. Comput. Phys.*, **110**, 68–81.
- Aihara, M. and H. Okamura, 1985: A numerical simulation of the finite-amplitude mountain waves using a meso-scale nonhydrostatic compressible model. *Pap. Meteor. Geophys.*, **36**, 119–135.
- Aranami, K. and J. Ishida, 2004: Implementation of two dimensional decomposition for JMA nonhydrostatic model. *CAS/JSC WGNE Res. Act. in Atmos. and Ocea. Modelling*, **34**, 0301–0302.
- Benard, P., J. Masek, and J. Vivoda, 2005: Stability of leap-frog constant-coefficients semi-implicit schemes for the fully elastic system of Euler equations. Case with orography. *Mon. Wea. Rev.*, **133**, 1065–1075.
- Benoit, R., M. Desgagne, P. Pellerin, S. Pellerin, Y. Chartier, and S. Desjardin, 1997: The Canadian MC2: A semi-lagrangian, semi-implicit wide-band atmospheric model suited for finescale process studies and simulation. *Mon. Wea. Rev.*, **125**, 2382–2415.
- Bouttier, F., 2003: Arome; a new operational meso-scale NWP system for Meteo-France. *CAS/JSC WGNE Res. Act. Atmos. Ocea. Modelling*, **33**, 0503–0504.
- Bubnova, R., G. Hello, P. Bénard, and J.-F. Geleyn, 1995: Integration of the fully-elastic equations cast in the hydrostatic pressure terrain-following coordinate in the framework of the ARPEGE/ALADIN NWP system. *Mon. Wea. Rev.*, **123**, 515–535.
- Carpenter, K.M., 1979: An experimental forecast using a non-hydrostatic mesoscale model. *Quart. J. Roy. Meteor. Soc.*, **105**, 629–655.
- Chen, D. and J. Xue, 2003: A brief introduction of the CMA's GRAPES project. *Proc., International Workshop on NWP models for heavy precipitation in Asia and Pacific Areas*. 142–146.
- Chen, D., X. Yang, H. Zhang, and J. Hu, 2003: Strategy for designing a non-hydrostatic multi-scale community model dynamic core. *Journal of Applied Meteorological Science*, **14**, 452–461. (in Chinese)
- Clark, T.L., 1977: A small scale numerical model

- using a terrain following coordinate system. *J. Comput. Phys.*, **24**, 186–215.
- Cote, J., S. Gravel, A. Methot, A. Patoine, M. Roch, and A. Staniforth, 1998a: The operational CMC-MRB global environmental multiscale (GEM) model. Part I: Design considerations and formulation. *Mon. Wea. Rev.*, **126**, 1373–1395.
- Cote, J., J.-G. Desmarais, S. Gravel, A. Methot, A. Patoine, M. Roch, and A. Staniforth, 1998b: The operational CMC-MRB global environmental multiscale (GEM) model. Part II: Results. *Mon. Wea. Rev.*, **126**, 1397–1418.
- Cotton, W.R. and G. Tripoli, 1978: Cumulus convection in shear flow—Three-dimensional numerical experiments. *J. Atmos. Sci.*, **35**, 1503–1521.
- Cotton, W.R., R.A. Pielke Sr., R.L. Walko, G.E. Liston, C.J. Tremback, H. Jiang, R.L. McAnelly, J.Y. Harrington, M.E. Nicholls, G.G. Carrio, and J.P. McFadden, 2003: RAMS 2001: Current status and future directions. *Meteor. Atmos. Phys.*, **82**, 5–29.
- Cullen, M.J.P., 1990: A test of a semi-implicit integration technique for a fully compressible non-hydrostatic model. *Quart. J. Roy. Meteor. Soc.*, **116**, 1253–1258.
- Cullen, M.J.P., 1993: The unified forecast/climate model. *Meteor. Mag.*, **122**, 81–94.
- Davies, T., M.J.P. Cullen, A.J. Malcolm, M.H. Mawson, A. Staniforth, A.A. White, and N. Wood, 2005: A new dynamical core for the Met Office's global and regional modelling of the atmosphere. *Quart. J. Roy. Meteor. Soc.*, **131**, 1759–1782.
- Deardorff, J.W., 1980: Stratocumulus-capped mixed layers derived from a three-dimensional model. *Bound.-Layer Meteor.*, **18**, 495–527.
- Doms, G. and U. Schaeffler, 1997: *The nonhydrostatic limited-area model LM (Lokal-Modell) of DWD. Part I: Scientific Documentation*. Deutscher Wetterdienst, 155 pp.
- Douglas, C.C., 1992: A review of numerous parallel multigrid methods. *SIAM News*, **25**, 20 pp.
- Du, J. and M.S. Tracton, 2001: Implementation of a real-time short-range ensemble forecasting system at NCEP: an update. Preprints, 9th Conference on Mesoscale Processes. Amer. Meteor. Soc., 355–356.
- Dudhia, J., 1993: A nonhydrostatic version of the Penn State-NCAR mesoscale model: Validation tests and simulation of an Atlantic cyclone and cold front. *Mon. Wea. Rev.*, **121**, 1493–1513.
- Dudhia, J. and J.F. Bresch, 2002: A global version of the PSU-NCAR mesoscale model. *Mon. Wea. Rev.*, **130**, 2989–3007.
- Durran, D.R., 1989: Improving the anelastic approximation. *J. Atmos. Sci.*, **46**, 1453–1461.
- Eito, H., C. Muroi, S. Hayashi, T. Kato, and M. Yoshizaki, 2004: High-resolution wide-range numerical simulation of cloud bands associated with the Japan Sea polar-air mass convergence zone in winter using a non-hydrostatic model on the Earth Simulator. *CAS/JSC WGNE Res. Act. Atmos. Ocea. Modelling*, **34**, 0507–0508.
- Fujibe, F., K. Saito, D.S. Wratt, and S.G. Bradley, 1999: A numerical study on the diurnal variation of low-level wind in the lee of a two-dimensional mountain. *J. Meteor. Soc. Japan*, **77**, 827–843.
- Fujita, T., 2003: Higher order finite difference schemes for advection of NHM. *Proceedings, International Workshop on NWP Models for Heavy Precipitation in Asia and Pacific Areas*, 78–81.
- Gal-Chen, T. and R.C.J. Somerville, 1975: On the use of a coordinate transform for the solution of the Navier-Stokes equation. *J. Comput. Phys.*, **17**, 209–228.
- Garratt, J.R. and R.J. Francey, 1978: Bulk characteristics of the heat transfer in the unstable baroclinic atmospheric boundary layer. *Bound.-Layer Meteor.*, **15**, 399–421.
- Goda, H. and K. Kurihara, 1991: Development of a nonhydrostatic model. Annual report of Numerical Prediction Division, JMA, **37**, 67–82. (in Japanese)
- Golding, B.W., 1990: The meteorological office mesoscale model. *Meteor. Mag.*, **119**, 81–96.
- Golding, B.W., 1992: An efficient non-hydrostatic forecast model. *Meteor. Atmos. Phys.*, **50**, 89–103.
- Gopalakrishnan, N. Surgi, R. Tuleya, and Z. Janjic, 2006: NCEP's Two-way-Interactive-Moving-Nest NMM-WRF modeling system for Hurricane Forecasting. Extended Abstracts, AMS 27th Conf. Hurricanes and Tropical Meteorology, 7A.3.
- Grell, G., J. Dudhia, and D. Stauffer, 1994: A description of the Fifth-Generation of the Penn State/NCAR Mesoscale Model (MM5). *NCAR Technical Note*, 138 pp.
- Hara, T., 2007: Implementation of improved Mellor-Yamada Level 3 scheme and partialcondensation scheme to JMANHM and their performance. *CAS/JSC WGNE Res. Act. in Atmos. and Ocea. Modelling*, **37**, 0407–0408.
- Hara, T., K. Aranami, R. Nagasawa, M. Narita, T. Segawa, D. Miura, Y. Honda, H. Nakayama, and K. Takenouchi, 2007: Upgrade of the operational JMA non-hydrostatic mesoscale model. *CAS/JSC WGNE Res. Act. in Atmos. and Ocea. Modelling*, **37**, 0511–0512.
- Heinze, T., P. Ripodas, D. Majewski, H. Frank, D. Liemann, B. Ritter, E. Roeckner, M. Giorgetta,

- L. Komblueh, P. Kom, H. Wan, and L. Bonaventura, 2005: ICON-Project: Development of a unified non-hydrostatic model. Proc., 6th International SRNWP-Workshop on Non-Hydrostatic Modelling.
- Hodur, R.M., 1997: The Naval Research Laboratory's Coupled Ocean/Atmospheric Mesoscale Prediction System (COAMPS). *Mon. Wea. Rev.*, **125**, 1414–1430.
- Honda, Y., M. Nishijima, K. Koizumi, Y. Ohta, K. Tamiya, T. Kawabata, and T. Tsuyuki, 2005: A pre-operational variational data assimilation system for a nonhydrostatic model at Japan Meteorological Agency: Formulation and preliminary results. *Quart. J. Roy. Meteor. Soc.*, **131**, 3465–3475.
- Hsu, W. and W. Sun, 2001: A time-split, forward-backward numerical model for solving a nonhydrostatic compressible system of equations. *Tellus*, **53A**, 279–299.
- Ikawa, M., 1988: Comparison of some schemes for nonhydrostatic models with orography. *J. Meteor. Soc. Japan*, **66**, 753–776.
- Ikawa, M. and K. Saito, 1991: Description of a nonhydrostatic model developed at the Forecast Research Department of the MRI. Technical Reports of the MRI, **28**, 238 pp.
- Ishida, J., 2007: Development of a hybrid terrain-following vertical coordinate for JMA Nonhydrostatic Model. *CAS/JSC WGNE Res. Act. in Atmos. and Ocea. Modelling*, **37**, 0309–0310.
- Ishida, J., T. Segawa, S. Ohmori, and H. Nakayama, 2005: The new mesoscale NWP model. *The 8<sup>th</sup> Generation NWP system, Textbook for NWP training, NPD/JMA*, **38**, 14–32. (in Japanese)
- Ishii, M. and K. Kurihara, 2002: Fast Poisson-Equation Solvers—An introduction to advanced methodologies: PSOR and Multigrid—. *Tenki*, **49**, 597–606. (in Japanese)
- Janjic, I.J., 2003: Nonhydrostatic model based on a new approach. *Meteor. Atmos. Phys.*, **82**, 271–285.
- Janjic, I.J., J.P. Gerrity, Jr., and S. Nickovic, 2001: An alternative approach to nonhydrostatic modeling. *Mon. Wea. Rev.*, **129**, 1164–1178.
- Juang, H.M., 2000: The NCEP Mesoscale Spectral Model: A Revised Version of the Nonhydrostatic Regional Spectral Model. *Mon. Wea. Rev.*, **128**, 2329–2362.
- Juang, H.M., 2003: The next generation of NCEP global atmospheric model. Proceedings, International Workshop on NWP Models for Heavy Precipitation in Asia and Pacific Areas, 154–158.
- Juang, H.M., S.Y. Hong, and M. Kanamitsu, 1997: The NCEP regional spectral model: an update. *Bull. Amer. Meteor. Soc.*, **78**, 2125–2143.
- Kain, J. and J. Fritsch, 1993: Convective parameterization for mesoscale models: The Kain-Fritsch scheme. *The Representation of Cumulus Convection in Numerical Models, Meteor. Monogr.*, **24**, 165–170.
- Kar, S.K., R.J. Purser, S. Gopalakrishnan, and G. Di-mego, 2005: A fully-implicit semi-Lagrangian nonhydrostatic model employing a pressure-hybrid vertical coordinate. *NCEP short contribution*, 25.2.
- Kato, T., 1995: Box-Lagrangian rain-drop scheme. *J. Meteor. Soc. Japan*, **73**, 241–245.
- Kato, T., 1998: Numerical simulation of the band-shaped torrential rain observed southern Kyushu, Japan on 1 August 1993. *J. Meteor. Soc. Japan*, **76**, 97–128.
- Kapitza, H. and D. Eppel, 1987: A 3-D poisson solver based on conjugate gradients compared to standard iterative methods and its performance on vector computers. *J. Comput. Phys.*, **68**, 474–484.
- Kawabata, T., H. Seko, K. Saito, T. Kuroda, K. Tamiya, T. Tsuyuki, Y. Honda, and Y. Wakazuki, 2007: An assimilation and forecasting experiment of the Nerima heavy rainfall with a cloud-resolving nonhydrostatic 4-Dimensional variational data assimilation system. *J. Meteor. Soc. Japan*, **85**, 255–276.
- Kikuchi, Y., 1975: Governing equations. *Separate volume of annual report of NPD*, **21**, 4–17. (in Japanese)
- Klemp, J.B. and R. Wilhelmson, 1978: The simulation of three-dimensional convective storm dynamics. *J. Atmos. Sci.*, **35**, 1070–1096.
- Klemp, J.B., W.C. Skamarock, and J. Dudhia, 2007: Conservative split-explicit time integration methods for the compressible nonhydrostatic equations. *Mon. Wea. Rev.* (in press)
- Koizumi, K., Y. Ishikawa, and T. Tsuyuki, 2005: Assimilation of precipitation data to JMA mesoscale model with a four-dimensional variational method and its impact on precipitation forecasts. *SOLA*, **1**, 45–48.
- Kumagai, Y., 2004a: Improvement of the land surface processes in JMANHM. *CAS/JSC WGNE Res. Act. in Atmos. and Ocea. Modelling*, **34**, 0419–0420.
- Kumagai, Y., 2004b: Implementation of a non-local like PBL scheme in JMANHM. *CAS/JSC WGNE Res. Act. in Atmos. and Ocea. Modelling*, **34**, 0417–0418.
- Lafore, J.P., J. Stein, N. Asencio, P. Bougeault, V. Ducrocq, J. Duron, C. Fischer, P. Hereil, P. Mascart, V. Masson, J.P. Pinty, J.L. Redelsperger, E. Richard, and J. Vila-Guerau de Arellano, 1998: The Meso-NH Atmospheric Simulation System. Part 1: adiabatic formula-

- tion and control simulations. *Ann. Geophysicae*, **16**, 90–109.
- Laprise, R., 1992: The Euler equations of motion with hydrostatic pressure as an independent variable. *Mon. Wea. Rev.*, **120**, 197–207.
- Li, P.W., W.K. Wong, and E.S.T. Lai, 2005: RAPIDS—A new rainstorm nowcasting system in Hong Kong. Proceeding, WWRP Symposium on Nowcasting and Very Short Range Forecasting, 7.17–24.
- Lin, Y.H., R.D. Farley, and H.D. Orville, 1983: Bulk parameterization of the snow field in a cloud model. *J. Climate Appl. Meteor.*, **22**, 1065–1092.
- Long, R.R., 1954: Some aspects of the flow of stratified fluids, II, Experiments with a two-fluid system. *Tellus*, **6**, 97–115.
- Louis, J.F., M. Tiedtke, and J.F. Geleyn, 1982: A short history of the operational PBL parameterization at ECMWF, Workshop on Planetary Boundary Layer Parameterization, ECMWF, England, 59–79.
- Majewski, D., D. Liermann, P. Prohl, B. Ritter, M. Buchhold, T. Hanisch, G. Paul, and W. Wergen, 2002: The operational global Icosahedral-Hexagonal gridpoint model GME: Description and high-resolution tests. *Mon. Wea. Rev.*, **130**, 319–338.
- Mannik, A. and R. Room, 2001: Nonhydrostatic adiabatic kernel for HIRLAM. Part II. Anelastic, hybrid-coordinate, explicit-Eulerian model. *HIRLAM Technical Reports*, **49**, 51 pp.
- McGregor, J., 1996: Semi-Lagrangian advection on conformal-cubic grids. *Mon. Wea. Rev.*, **124**, 1311–1322.
- Miyoshi, T. and K. Aranami, 2006: Applying a four-dimensional local ensemble transform Kalman filter (4D-LETKF) to the JMA nonhydrostatic model (NHM). *SOLA*, **2**, 128–13.
- Murakami, M., 1990: Numerical modeling of dynamical and microphysical evolution of an isolated convective cloud—the 19 July 1981 CCOP cloud—. *J. Meteor. Soc. Japan*, **68**, 107–128.
- Muroi, C., 2006: Development of a global nonhydrostatic model with cubic grids. *Report on effects of ocean-atmosphere interaction on prediction with cloud resolving models. Advance Earth Science and Technology Organization*, 33–37. (in Japanese)
- Muroi, C., K. Saito, T. Kato, and H. Eito, 1999: Development of the MRI/NPD nonhydrostatic model, Proc. Workshop on Mesoscale Numerical Weather Prediction and its Application, 83–86.
- Nagasawa, R. and H. Kitagawa, 2005: Modification of radiation scheme of JMA-NHM. Proc. Autumn Conf. JMSJ, **87**, B403. (in Japanese)
- Nakanishi, M. and H. Niino, 2004: An improved Mellor-Yamada level 3 model with condensation physics: Its design and verification. *Bound.-Layer Meteor.*, **112**, 1–31.
- Nakanishi, M. and H. Niino, 2006: An improved Mellor-Yamada level-3 model: Its numerical stability and application to a regional prediction of advection fog. *Bound.-Layer Meteor.*, **119**, 397–407.
- Narita, M., 2006: On the modification of Kain-Fritsch convective parameterization scheme in JMA nonhydrostatic model. Proceedings, 8<sup>th</sup> Workshop on nonhydrostatic models. 31–32. (in Japanese)
- Ogura, M., 1969: A direct method of Poisson equation by dimension reduction method. *J. Atmos. Sci.*, **47**, 319–323.
- Ogura, Y. and N.A. Phillips, 1962: Scale analysis of deep and shallow water convection in the atmosphere. *J. Atmos. Sci.*, **19**, 173–179.
- Ohmori, S. and Y. Yamada, 2006: Development of cumulus parameterization scheme in the nonhydrostatic mesoscale model at the Japan Meteorological Agency. *CAS/JSC WGNE Res. Act. in Atmos. and Ocea. Modelling*, **35**, 0421–0422.
- Orlanski, I., 1976: A simple boundary condition for unbounded hyperbolic flows. *J. Comput. Phys.*, **21**, 251–269.
- Pielke, R.A., W.R. Cotton, R.L. Walko, C.J. Tremback, W.A. Lyons, L.D. Grasso, M.E. Nicholls, M.D. Moran, D.A. Wesley, T.J. Lee, and J.H. Copeland, 1992: A comprehensive meteorological modeling system-RAMS. *Meteor. Atmos. Phys.*, **49**, 69–91.
- Purser, J.R., Z.I. Janjic, and T.L. Black, 2005: A bicylindrical “Yin-Yang” global grid geometry applied to the NCEP Nonhydrostatic Mesoscale Model. Extended Abstract, AMS 21st Conf. on Weather Analysis and Forecasting.
- Qian, J.H., F.H.M. Semmazi, and J.S. Scroggs, 1998: A global nonhydrostatic semi-Lagrangian atmospheric model with orography. *Mon. Wea. Rev.*, **126**, 747–771.
- Rancic, M., R.J. Purser, and F. Mesinger, 1996: A global shallow-water model using an expanded spherical cube: Gnomonic versus conformal coordinates. *Quart. J. Roy. Meteor. Soc.*, **122**, 959–982.
- Redelsperger, J.L. and G. Sommeria, 1986: Three-dimensional simulation of a convective storm: Sensitivity studies on subgrid parameterization and spatial resolution. *J. Atmos. Sci.*, **43**, 2619–2635.
- Robert, A.J., 1966: The integration of low order spectral form of the primitive meteorological equations. *J. Atmos. Sci.*, **44**, 237–245.

- Room, R., A. Mannik, and A. Luhamaa, 2006: Non-hydrostatic adiabatic kernel for HIRLAM Part IV Semi-implicit semi-Lagrangian scheme. *HIRLAM Technical Reports*, **65**, 42 pp.
- Saito, K., 1993: Numerical simulation of mesoscale wind field with a nonhydrostatic model (3)—in the case of a semi-implicit elastic model. Proc. Autumn Conf, MSJ, **64**, C305.
- Saito, K., 1994: A numerical study of the local down-slope wind “Yamaji-kaze” in Japan. Part 3: Numerical simulation of the 27 September 1991 windstorm with a non-hydrostatic multi-nested model. *J. Meteor. Soc. Japan*, **72**, 301–329.
- Saito, K., 1997: Semi-implicit fully compressible version of the MRI mesoscale nonhydrostatic model—Forecast experiment of the 6 August 1993 Kagoshima torrential rain—. *Geophys. Mag. Ser. 2*, **2**, 109–137.
- Saito, K., 1999: Classification of nonhydrostatic model. *Meteor. Res. Notes*, **196**, 19–35. (in Japanese)
- Saito, K., 2001: A global version of the Meteorological Research Institute/Numerical Prediction Division nonhydrostatic model. *CAS/JSC WGNE Res. Act. in Atmos. and Ocea. Modelling*, **31**, 6.20–6.21.
- Saito, K., 2003a: Time-splitting of advection in the JMA Nonhydrostatic Model. *CAS/JSC WGNE Res. Act. in Atmos. and Ocea. Modelling*, **33**, 0315–0316.
- Saito, K., 2003b: Dynamical process in the nonhydrostatic model. *Separate volume of annual report of NPD*, **49**, 16–25. (in Japanese)
- Saito, K., 2004: Direct evaluation of the buoyancy and consideration of moisture diffusion in the continuity equation in the JMA nonhydrostatic model. *CAS/JSC WGNE Res. Act. in Atmos. and Ocea. Modelling*, **34**, 0525–0526.
- Saito, K., G. Doms, U. Schaeffer, and J. Steppeler, 1998: 3-D mountain waves by the Lokal-Modell of DWD and the MRI-mesoscale nonhydrostatic model. *Pap. Meteor. Geophys.*, **49**, 7–19.
- Saito, K. and T. Kato, 1999: The MRI mesoscale nonhydrostatic model. *Meteor. Res. Notes*, **196**, 169–195. (in Japanese)
- Saito, K., T. Keenan, G. Holland, and K. Puri, 2001a: Numerical simulation of tropical diurnal thunderstorms over the Maritime Continent. *Mon. Wea. Rev.*, **129**, 378–400.
- Saito, K., T. Kato, H. Eito, and C. Muroi, 2001b: Documentation of the Meteorological Research Institute/Numerical Prediction Division unified nonhydrostatic model. *Tech. Rep. MRI*, **42**, 133 pp.
- Saito, K. and J. Ishida, 2005: Implementation of the Targeted Moisture Diffusion to JMA-NHM. *CAS/JSC WGNE Res. Act. in Atmos. and Ocea. Modelling*, **35**, 0517–0518.
- Saito, K., T. Fujita, Y. Yamada, J. Ishida, Y. Kumagai, K. Aranami, S. Ohmori, R. Nagasawa, S. Kumagai, C. Muroi, T. Kato, H. Eito, and Y. Yamazaki, 2006: The operational JMA non-hydrostatic model. *Mon. Wea. Rev.*, **134**, 1266–1298.
- Satoh, M., H. Tomita, H. Miura, S. Iga, and T. Nasuno, 2005: Development of a global cloud resolving model—a multi-scale structure of tropical convections—. *J. Earth Simulator*, **3**, 11–19.
- Satomura, T., 1989: Compressible flow simulation on numerically generated grids. *J. Meteor. Soc. Japan*, **67**, 473–482.
- Satomura, T., T. Iwasaki, K. Saito, C. Muroi, and K. Tsuboki, 2003: Accuracy of terrain following coordinates over isolated mountain: Steep mountain Model intercomparison project (St-MIP). Annuals, Disas. Prev. Res. Inst., Kyoto University, **46**, 337–346.
- Schar, C., D. Leuenberger, O. Fuhrer, D. Luthi, and C. Girard, 2002: A new terrain-following vertical coordinate formulation for atmospheric prediction models. *Mon. Wea. Rev.*, **130**, 2459–2480.
- Segawa, T. and D. Miura, 2006: Statistical verification of MSM. *Textbook for NWP training, NPD/JMA*, **39**, 59–83. (in Japanese)
- Seko, H., K. Saito, M. Kunii, T. Hara, M. Kyouda, and M. Yamaguchi, 2007: Japan area mesoscale ensemble experiments using JMANHM. *CAS/JSC WGNE Res. Act. in Atmos. and Ocea. Modelling*, **37**, 0531–0532.
- Sherman, C.A., 1978: A mass-consistent model for wind fields over complex terrain. *J. Appl. Meteor.*, **17**, 312–319.
- Skamarock, W.C. and J.B. Klemp, 1992: The stability of time-split numerical methods for the hydrostatic and the nonhydrostatic elastic equations. *Mon. Wea. Rev.*, **120**, 2109–2127.
- Skamarock, W.C. and J.B. Klemp, 2007: Numerical techniques for high-resolution NWP models. *J. Comput. Phys.* (in press)
- Skamarock, W.C., J.B. Klemp, J. Dudhia, D.O. Gill, D.M. Barker, W. Wang, and J.G. Powers, 2005: A Description of the Advanced Research WRF Version 2. *NCAR Tech. Note*, **468**, 88 pp.
- Sommeria, G., 1976: Three-dimensional simulation of turbulent processes in an undisturbed trade wind boundary layer. *J. Atmos. Sci.*, **33**, 216–241.
- Soong, S.T. and Y. Ogura, 1980: Response of trade wind cumuli to large-scale processes. *J. Atmos. Sci.*, **37**, 2035–2050.
- Staniforth, A. and J. Cote, 1991: Semi-Lagrangian

- Integration Schemes for Atmospheric Models—A Review. *Mon. Wea. Rev.*, **119**, 2206–2223.
- Staniforth, A., A. White, N. Wood, J. Thuburn, M. Zerroukat, E. Cordero et al., 2002: Unified Model Documentation Paper, 15, Joy of UM 5.3—Model formulation, *UKMO*.
- Steppeler, J., R. Hess, U. Schättler, L. Bonaventura, 2003a: Review of numerical methods for non-hydrostatic weather prediction models. *Meteor. Atmos. Phys.*, **82**, 287–301.
- Steppeler, J., U. Schättler, H.W. Bitzer, A. Gassmann, U. Damrath, and G. Gregoric, 2003b: Meso gamma scale forecasts by nonhydrostatic model LM. *Meteor. Atmos. Phys.*, **82**, 75–96.
- Steppeler, J., H.W. Bitzer, Z. Janjic, U. Schättler, P. Prohl, U. Gjertsen, L. Torrisi, J. Parfiniecicz, E. Avgoustogloy, and U. Damrath, 2006: Prediction of clouds and rain using a z-coordinate nonhydrostatic model. *Mon. Wea. Rev.*, **134**, 3625–3643.
- Sun, W.Y. and C.Z. Chang, 1986: Diffusion model for a convective layer. Part I: Numerical simulation of convective boundary layer. *J. Climate Appl. Meteor.*, **25**, 1445–1453.
- Tao, W.K., 2003: Goddard Cumulus Ensemble (GCE) Model: Application for understanding precipitation processes. *Meteor. Monogr.*, **29**, 107–138.
- Tao, W.K. and J. Simpson, 1993: The Goddard cumulus ensemble model. Part 1: Model description. *Terr. Atmos. Ocea. Sci.*, **4**, 35–72.
- Takahashi, K., X. Peng, K. Komine, M. Ohdaira, K. Goto, M. Yamada, H. Fuchigami, and T. Sugimura, 2005: “Non-hydrostatic atmospheric GCM development and its computational performance”, Use of High Performance computing in meteorology, *Walter Zwiefelhofer and George Mozdzynski Eds.*, *World Scientific*, 50–62.
- Takahashi, T. 1975: Tropical showers in an axisymmetric cloud model. *J. Atmos. Sci.*, **32**, 1318–1330.
- Takeda, T., 1971: Numerical simulation of a precipitating convective cloud: the formation of a “long-lasting” cloud. *J. Atmos. Sci.*, **28**, 350–376.
- Tanguay, M.A., A. Robert, and R. Laprise, 1990: A semi-implicit semi-Lagrangian fully compressible regional forecast model. *Mon. Wea. Rev.*, **118**, 1970–1980.
- Tapp, M.C. and P.W. White, 1976: A non-hydrostatic mesoscale model. *Quart. J. Roy. Meteor. Soc.*, **102**, 277–296.
- Thomas, S., C. Girard, G. Doms, and U. Schättler, 1999: Semi-implicit scheme for the DWD Lokal-Modell. *Meteor. Atmos. Phys.*, **73**, 105–125.
- Tomita, H. and M. Satoh, 2004: A new dynamical framework of nonhydrostatic global model using the icosahedral grid. *Fluid Dyn. Res.*, **34**, 357–400.
- Tripoli, G.J. and W.R. Cotton, 1982: The Colorado State University three-dimensional cloud/mesoscale model—1982. Part I: General theoretical framework and sensitivity experiments. *J. Rech. Atmos.*, **16**, 185–220.
- Tsuboki, K., 2006: High-resolution simulations of high-impact weather systems using the cloud-resolving model on the Earth Simulator. *High Resolution Numerical Modeling of the Atmosphere and Ocean*. Springer, New York. (in press)
- Tsuboki, K. and A. Sakakibara, 2002: Large-scale parallel computing of Cloud Resolving Storm Simulator. *High Performance Computing*, 243–259.
- Uden, P., L. Rontu, H. Jarvinen, P. Lynch, J. Calvo, G. Cats, J. Cuxart, K. Eerola, C. Fortelius, J. Moya, C. Jones, G. Lenderlink, A. McDonald, R. McGrath, B. Navasques, N. Nielsen, V. Odegaard, E. Rodriguez, M. Rummukainen, R. Room, K. Sattler, B. Sass, H. Savijarvi, B. Schreur, R. Sigg, H. The, and A. Tijn, 2002: *HIRLAM-5 Scientific Documentation*, Sweden, 144 pp.
- Weiss, S.J., D.R. Bright, J.S. Kain, J.J. Levit, M. Pyle, Z. Janjic, B.S. Ferrier, and J. Du, 2006: Complementary Use of Short-Range Ensemble and 4.5 km WRF-NMM Model Guidance for Severe Weather Forecasting at the Storm Prediction Center. Extended Abstracts, AMS 23rd Conf. on Severe Local Storms, 8.5.
- Wong, M.C., W.K. Wong, and E.S.T. Lai, 2006: From SWIRLS to RAPIDS: Nowcast applications development in Hong Kong, WMO PWS Workshop on Warnings of Real-Time Hazards by Using Nowcasting Technology, Sydney, 9–13 October 2006. (available from: <http://www.weather.gov.hk/publica/reprint/r677.pdf>)
- Xie, D. and L. Adams, 1999: New parallel SOR method by domain partitioning, *SIAM J. Sci. Comput.*, **20**, 2261–2281.
- Xue, M., K.K. Droegemeier, V. Wong, A. Shapiro, and K. Brewster, 1995: Advanced Regional Prediction System, Version 4.0. Center for Analysis and Prediction of Storms, University of Oklahoma, 380 pp.
- Xue, M., D. Wang, J. Gao, K. Brewster, and K.K. Droegemeier, 2003: The Advanced Regional Prediction System (ARPS), storm-scale numerical weather prediction and data assimilation. *Meteor. Atmos. Phys.*, **82**, 139–170.
- Yamada, Y., 2003: Introduction to the Kain-Fritsch scheme. *Separate volume of annual report of NPD*, **49**, 84–89. (in Japanese)

- Yamasaki, M., 1975: A numerical experiment of the interaction between cumulus convection and large-scale motion. *Pap. Meteor. Geophys.*, **26**, 63–91.
- Yamasaki, M., 1984: Dynamics of convective clouds and “CISK” in vertical shear flow—with its application to easterly waves and squall-line systems. *J. Meteor. Soc. Japan*, **62**, 833–863.
- Yamazaki, Y. and K. Saito, 2004: Implementation of the Cylindrical Equidistant Projection for the Non-Hydrostatic Model of the Japan Meteorological Agency. *CAS/JSC WGNE Res. Act in Atmos. and Ocea. Modelling*, **34**, 0327–0328.
- Yeh, K.-S., J. Cote, S. Gravel, A. Methot, A. Patoiné, M. Roch, and A. Staniforth, 2002: The operational CMC-MRB global environmental multi-scale (GEM) model. Part III: Non-hydrostatic Formulation. *Mon. Wea. Rev.*, **130**, 339–350.
- Yoshimura, H. and T. Matsumura, 2005: A Two-Time-Level Vertically-Conservative Semi-Lagrangian Semi-Implicit Double Fourier Series AGCM. *CAS/JSC WGNE Res. Act. Atmos. Ocea. Model.*, **35**, 0325–0326.
- Yoshizaki, M., 1988: Documentation of a cloud model for numerical experiment of orographic precipitation. Ocean Research Institute, Univ. Tokyo, 77 pp. (in Japanese)
- Zou, X., W. Huang, and Q. Xiao, 1998: A user’s guide to the MM5 adjoint modeling system. *NCAR Tech. Note*. NCAR/TN-437+IA, 98 pp.